7. Systems and Components

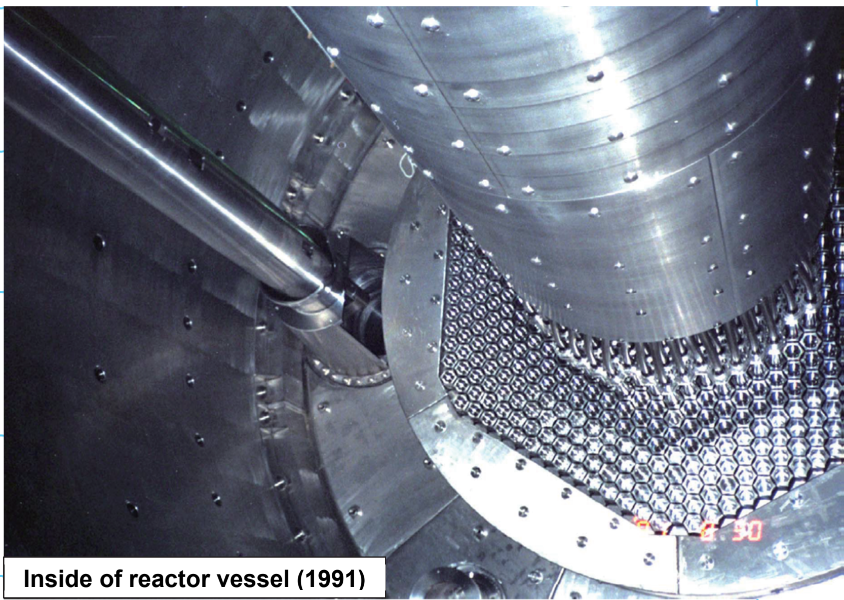

Inside of reactor vessel (1991)

- **Monju is a loop-type FR, adopting a hot-type reactor vessel, horizontal pipe routing at high elevation in the primary heat transport system, and helical-coil-type steam generators, to realize a simple and highly efficient reactor system while ensuring safety and reliability.**
- **The major sodium components are used under low pressures, high temperatures, and significant thermal load during transients. Thus, various mockup tests and thermal-hydraulics tests were conducted to clarify the mechanical behaviors of the components, such as sodium thermal hydraulic behaviors, the occurrence of convection in narrow gaps, and temperature stratification and striping.**
- **The major components were manufactured and installed as scheduled with high precision based on trial-manufacturing experience. In particular, the reactor vessel, featuring a large thin-walled cylindrical geometry, was manufactured with careful control of strain using unique large-scale vertical manufacturing equipment.**
- **Design and manufacturing technologies for the reactor systems and components were established by demonstrating their as-designed performances through the commissioning tests up to the 40% power.**

7.1 Plant overview

Monju reactor and cooling systems are shown in Fig. 7-1. Monju is a loop-type reactor with three independent sodium cooling systems. Each of the cooling systems consists of a primary heat transport system (PHTS) and a secondary heat transport system (SHTS), and heat is transferred to the power-generation steam turbine of a water-steam system via the steam generators (SGs).

The primary sodium flows into the reactor vessel (RV) from the bottom shell at 397°C, flows out from the upper shell at 529°C after being heated in the reactor core, and then exchanges heat with the secondary sodium in the intermediate heat exchanger (IHX). The secondary sodium is heated from 325°C to 505°C and exchanges heat with water and steam in the SGs to generate superheated steam of 483°C and a pressure of 127 kg/cm^{2}G that is supplied to the turbine generator.

The reactor system consists of:

- An RV that contains a core,
- A guard vessel to maintain the coolant level for safe core cooling in case of sodium leak from the PHTS piping,
- A shield plug that shields radiation and heat from the core and maintains an argon gas atmosphere above the sodium surface,
- Core internals that support the core and provide flow distribution for each core component, and
- An upper core structure that supports control rod drive mechanisms (CRDMs) and core instrumentation wells.

The cooling system consists of the following:

- PHTS equipment (circulation pump, IHX, guard vessel, etc.),
- SHTS equipment (circulation pump, SG, etc.),
- An auxiliary cooling system (air cooler, etc.),
- A sodium-water reaction product container,
- Reactor cooling system auxiliary equipment (auxiliary primary sodium equipment, auxiliary secondary sodium equipment, maintenance cooling system equipment, primary and secondary argon gas system equipment, etc.), and
- Water-steam system equipment including steam turbines.

The design features, R&D activities, and manufacturing and installation of the major systems and components of Monju are described in the following sections, together with those of the fuel handling and storage system not shown in Fig. 7-1.

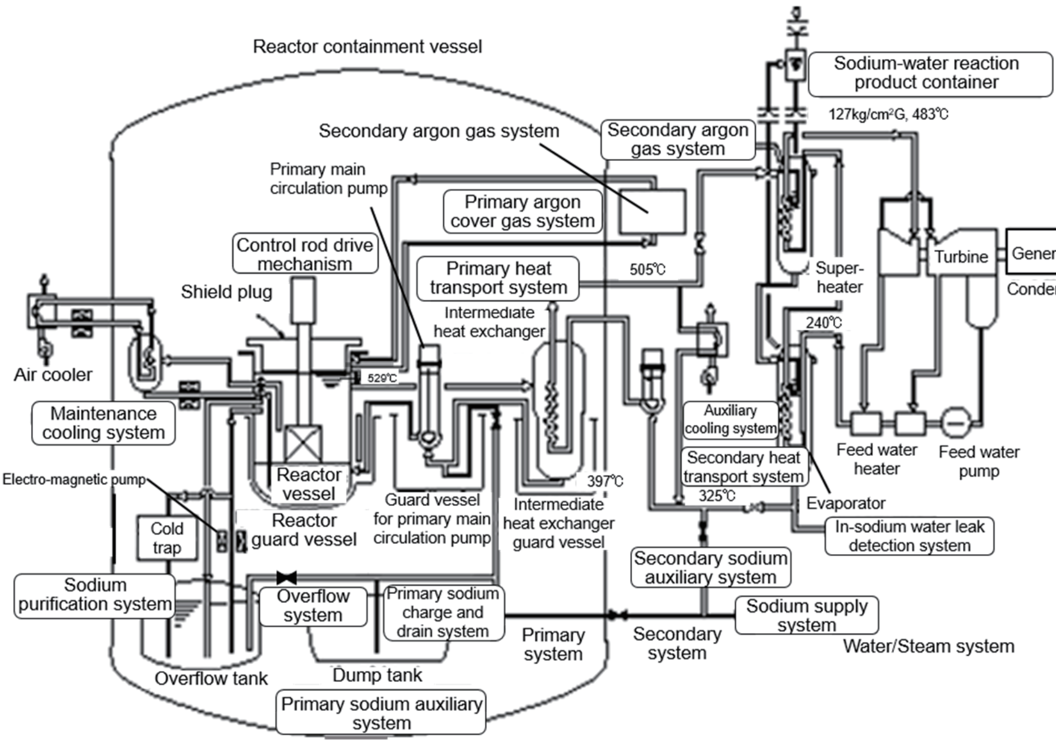

Fig.7-1 Reactor and cooloing system of Monju

7.2 Reactor structure

Reactor structure detail is shown in Fig. 7-2. The RV contains the core and core internals, and the reactor guard vessel encloses the RV and lower part of PHTS piping. The CRDMs and a refueling system are installed on the shield plugs (fixed plug and rotating plug).

7.2.1 Reactor vessel

Major specifications of the RV are listed in Table 7-1. The RV is a large, SUSF304 (forged material), thin-walled, cylindrical vessel with an outer diameter of 7 m, a height of 18 m, and a thickness of 50 mm. The vessel is supported at the upper flange, and it has a seismic support on the bottom end plate. The core internals (material: SUS304 and SUSF304) constitute the pressure and temperature boundary inside the RV (the upper plenum is at high temperature and low pressure, and the lower plenum at low temperature and high pressure). They also form flow paths to supply coolant to the fuel subassembly and other core elements (Figs. 7-3 and 7-4). The flow rate required for cooling each core element is supplied from the high and low pressure plenums below the core. The RV inlet and outlet coolant temperatures at the rated power operation are 397°C and 529°C, respectively. The space above the sodium level in the RV is filled with argon cover gas. The sodium level is maintained within a specified range by the primary sodium overflow system.

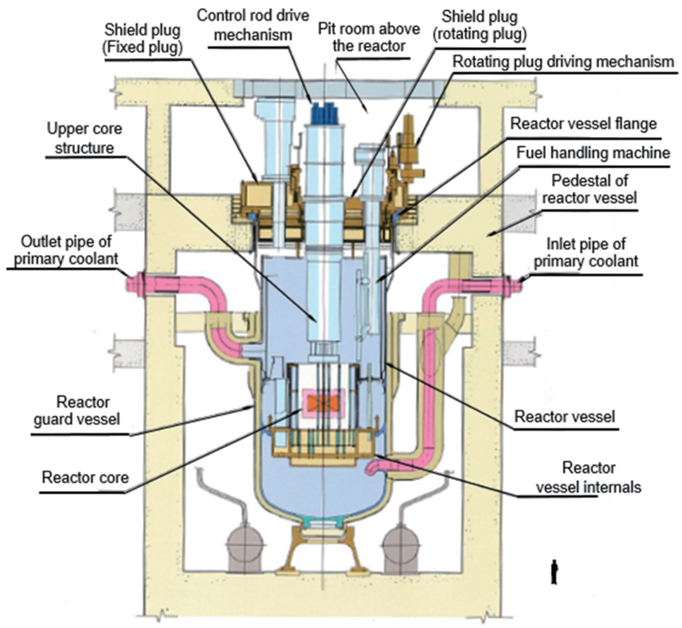

Fig.7-2 Reactor structure

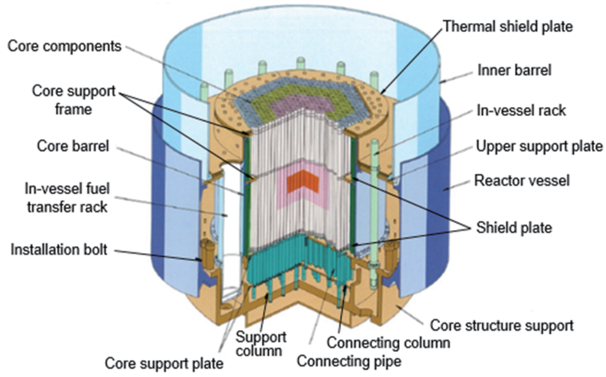

Fig.7-3 Core internal structure

Table 7-1 Major specifications of reactor vessel

Type	Specifications*
Maximum pressure and temperature Lower plenum pressure temperature Upper plenum pressure temperature	 10 kg/cm^{2}G 420°C 2 kg/cm^{2}G 550°C
Operating pressure (at rated power) RV inlet RV outlet	 ~6 kg/cm^{2}G ~1 kg/cm^{2}G
Operating temperature (at rated power) RV inlet RV outlet	 ~397°C ~529°C
Major dimensions Inner diameter Total height Shell thickness	 ~7.1 m ~17.8 m 50 mm
Material	Austenitic stainless steel (SUSF304)

*Thin-walled, cylindrical vessel equipped with a bottom end plate

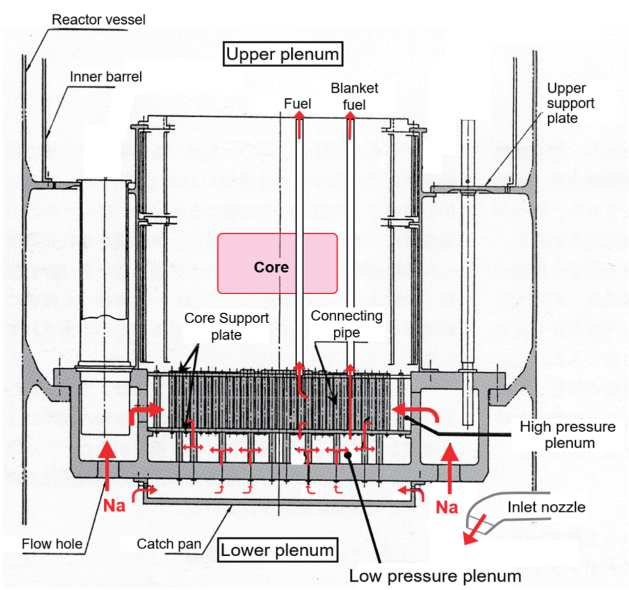

Fig.7-4 Coolant flow paths to the reactor core

(1) Design features of RV

The Monju RV was designed with careful consideration of the characteristics of sodium-cooled FRs, compared with LWRs, such as lower pressures, higher temperatures, and hence more severe thermal stress during plant thermal transients. In particular, design measures such as thin-walled piping must be taken to cope with thermal stresses. On the other hand, rigid structures were requested from perspective of the seismic design. The important task in RV design, therefore, was to harmonize and optimize these two competing requirements.

Adoption of the "hot-vessel-type" structure is another unique feature of the Monju RV. It makes the RV structure simple and compact by not installing a function to cool the RV wall, which was generally adopted in tank-type FRs.

Various R&D activities related to thermal hydraulics, seismic design, material strength, etc. were performed to establish the design methods and optimize the structure.

Major R&D achievements are summarized below.

a) Selection of structural materials

Since the main load on the RV is thermal stress, austenitic stainless steel (SUSF304) was selected to prevent excessive inelastic deformation caused by thermal stress and creep fatigue fracture. The material's favorable properties include elevated-temperature strength (creep strength, creep fatigue strength, etc.), corrosion resistance in sodium, and resistance to neutron irradiation.

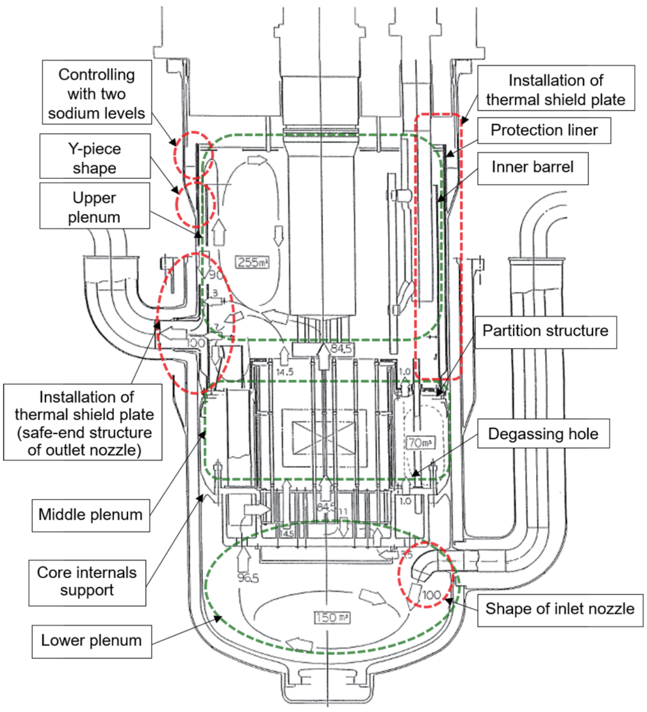

Fig.7-5 Measures against thermal shock

b) Measures against thermal transients near sodium surface

Upon reactor startup or shutdown, core outlet coolant temperature change is large and rapid, while that in the cover gas layer is small and slow. This difference together with the small heat-transfer rate from the gas to the RV wall would cause steep temperature gradient in the axial direction near the sodium surface in the RV. This would generate large thermal stress in the RV wall. As a measure to prevent creep fatigue damage due to this thermal stress, a two-sodium-level system with a protection liner was developed (Fig. 7-5). This system prevents the generation of excessive thermal stress in the RV wall by controlling the sodium level outside the protection liner. For example, in the case of reactor startup, the sodium level outside is initially set to the same level as inside during the first half period of the reactor startup procedure, and then the sodium level is lowered by about 0.6 m. This operating procedure would shift the peak position of the thermal stress with time to adequately mitigate overall influence on the RV.

c) Measures against thermal shock

Upon a reactor trip, a large thermal shock may develop in the RV wall and outlet nozzle because of rapid decrease in core outlet sodium temperature. To mitigate the shock, the inner barrel was installed in the upper plenum, and the RV wall was entirely covered with the thermal shield plate from the top of the inner side of the protection liner to the upper part of the inner barrel support. In the middle plenum, a measure was also taken to smoothen the axial temperature distribution in the RV wall by providing a bypass flow from the lower plenum through the degassing holes (Fig. 7-5).

d) Seismic support allowing thermal expansion

To enhance seismic capability, the lower support was attached below the bottom end plate of the RV and was fitted in the lower support structure on the RV cavity floor to constrain horizontal RV movement during earthquake (Fig. 7-6). This seismic support structure was designed to appropriately accommodate thermal expansion associated with power increase as well.

e) Measure to prevent fuel subassembly lifting

To prevent the lifting of the core fuel subassemblies due to upward coolant flow, a hydraulic hold-down mechanism is provided. Namely, a downward hold-down force is ensured by supplying coolant from the high-pressure plenum to the core fuel subassemblies. A part of the coolant flows downward to the low-pressure plenum located below the subassemblies, as shown in Fig. 7-4.

(2) R&D on RV

Upon a reactor trip, the core flow rate rapidly decreases to 10% of the rated value, and low-temperature sodium from the core flows into the stagnant high-temperature sodium region in the upper plenum. This creates the low-temperature sodium layer below a high-temperature layer, and the boundary between the two layers gradually rises. This phenomenon is called "thermal stratification" and may cause large thermal stress caused by the temperature gradient along the stratification boundary (Fig. 7-7).

A similar thermal stratification phenomenon is seen at the RV outlet nozzle, where a stagnant high-temperature sodium region appears in the upper layer and a low-temperature sodium flow through the inner barrel flow holes appears in the lower layer.

These phenomena were experimentally simulated by water and sodium thermal-hydraulic tests. The obtained data were used in design improvement to mitigate the influence of the thermal stratification as follows:

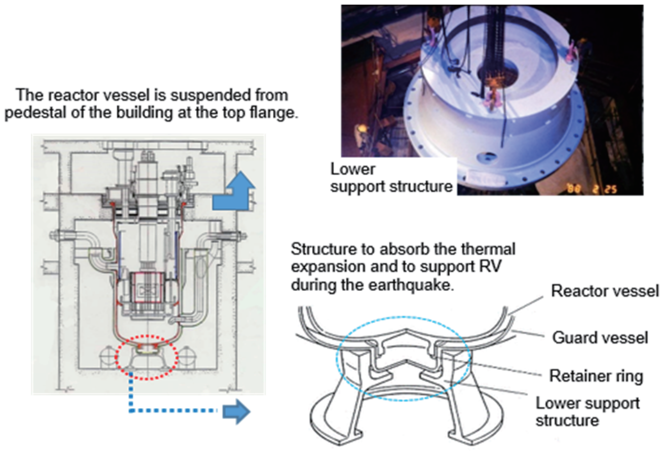

Fig.7-6 Seismic support structure

- The stress at the Y-piece of the RV is mitigated by increasing the inner barrel height by 1 m,
- The thermal stratification in the upper plenum is eliminated in a short time by generating a circulating flow using the sodium pumped up from the overflow system, and
- The local thermal stratification at the outlet nozzle is mitigated by providing the flow holes in the upper and lower parts of the inner barrel.

(3) Manufacturing and installation of RV

Ring forging was adopted in the manufacture of the RV shell for the purposes of avoiding a longitudinal weld line near sodium surface where large thermal stress may occur, minimizing the number of weld lines from the perspectives of in-service inspection and reliability, and obtaining geometrical accuracy including roundness.

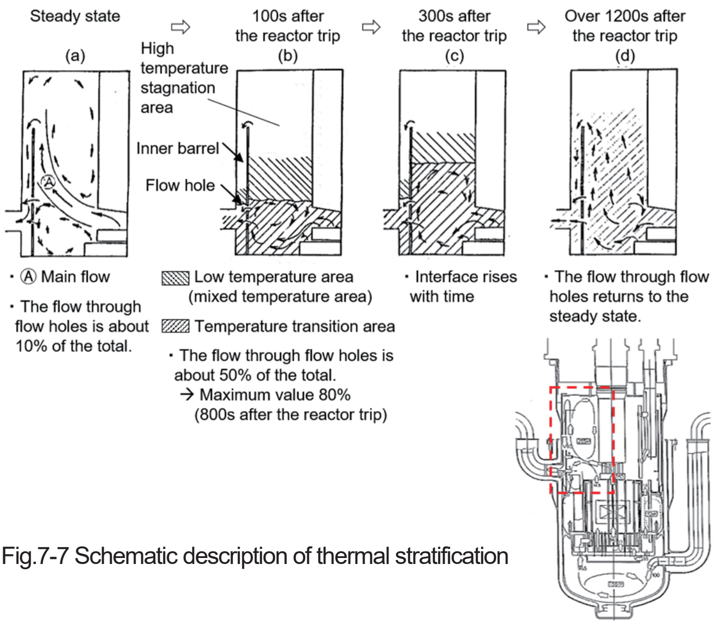

Fig.7-7 Schematic description of thermal stratification

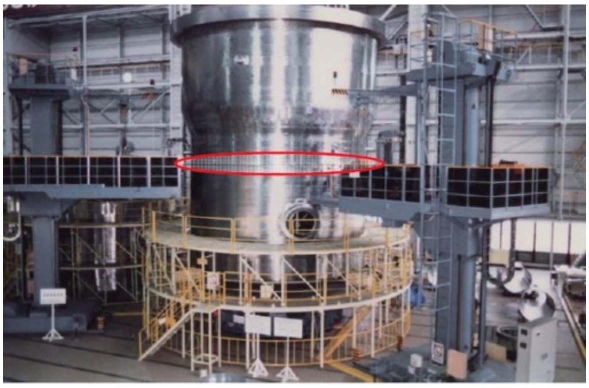

Photo 7-1 High-quality, low-strain automatic welding

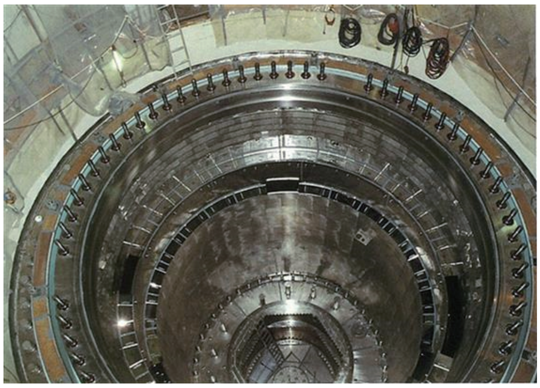

Photo 7-2 Inner barrel after installation

The forging of such a large-diameter thin-walled shell as the RV had never been experienced before. Furthermore, the weight of the used stainless steel ingot was about twice the largest ingot of 120 tons ever produced. Since ingot quality may significantly affect product quality, large ingot production technology with a high level of cleanliness was further advanced using a special method called “unified pouring”, in which ununiformed solidification was prevented by pouring molten steel heats in multiple steps, gradually decreasing the concentration. As a result, high-quality steel ingot was successfully produced.

In assembling the ring parts of the RV, a large-scale welding machine capable of high-quality and low-strain automatic welding was developed, and the parts were assembled vertically to minimize deformation and to ensure good welding workability, realizing sufficient accuracy in the manufacturing and installation (Photo 7-1).

After installation, the straightness of the RV from the support flange to the lower support was confirmed within 1 mm for the total height of 18 m. Concerning the installation accuracy of core internals, which is important for control rod insertability, the misalignment of the outermost control rod guide tubes is at most 1.9 mm at the upper core support frame level, sufficiently satisfying the design allowance. An internal view of the inner barrel after installation is shown in Photo 7-2.

(4) Design validation in SST

Axial temperature distribution in the upper plenum was measured in the reactor trip test from 40% power level performed during the SST in 1995. It was observed that temperature dropped after reactor trip more sharply in the lower elevations. The change in the temperature distribution is successfully simulated by analysis (Fig. 7-8). In addition, this result on the thermal stratification is well within the range postulated in the design. The data obtained are internationally utilized in the IAEA benchmark analysis[7-1].

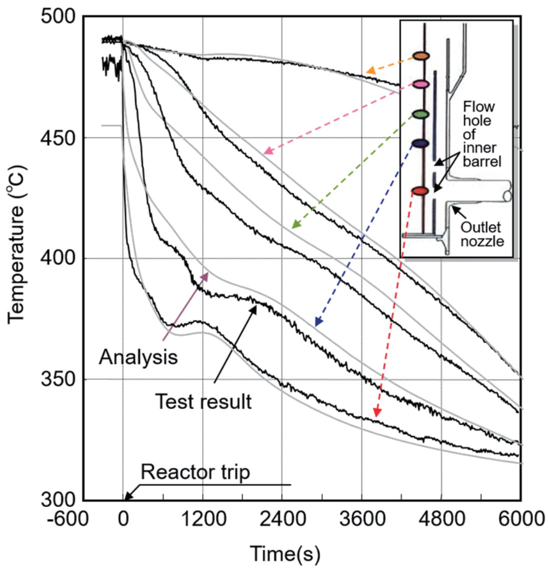

Fig.7-8 Temperature change in the upper plenum after reactor trip

7.2.2 Shield plug

The structure and the major specifications of the shield plug are shown in Fig. 7-9 and Table 7-2, respectively. The shield plug installed in the upper part of the RV is of a single rotating type and consists of the fixed plug and rotating plug. Each plug consists of the upper plate, shield shell, and dip plate. The dip plate was designed to suppress ruffling of sodium surface in the RV during power operation. The fixed plug has a maximum diameter of 9.5 m and a total height of 2.0 m.

Table 7-2 Major specifications of shield plug

	Fixed plug	Rotating plug
(1) Type	Single rotating plug	
(2) Major dimensions (upper plate)		
Outer diameter (m)	~9.5	~5.3
Shell thickness (mm)	~70	~60
Total height (m)	~2.0	~1.5
(3) Weight of plug (t)	~570	~270
(4) Main materials		
Upper plate	SVG42, SM41B	SFVQ1A, SM41B, SVG42
Shield shell	SUS304, SFVQ1A	
Shield layer	SUS304, SM41B, SS41	
Thermal shield layer	SUS304	
Dipped plate	SUS304	
(5) Sealing method	Low melting point alloy Synthetic rubber (elastomer seal)	
(6) Rotation speed of rotating plug (rpm)	-	~0.1

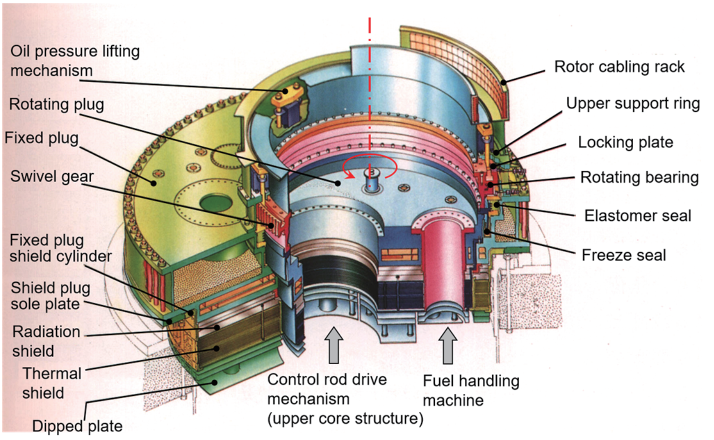

Fig.7-9 Structure of shield plug

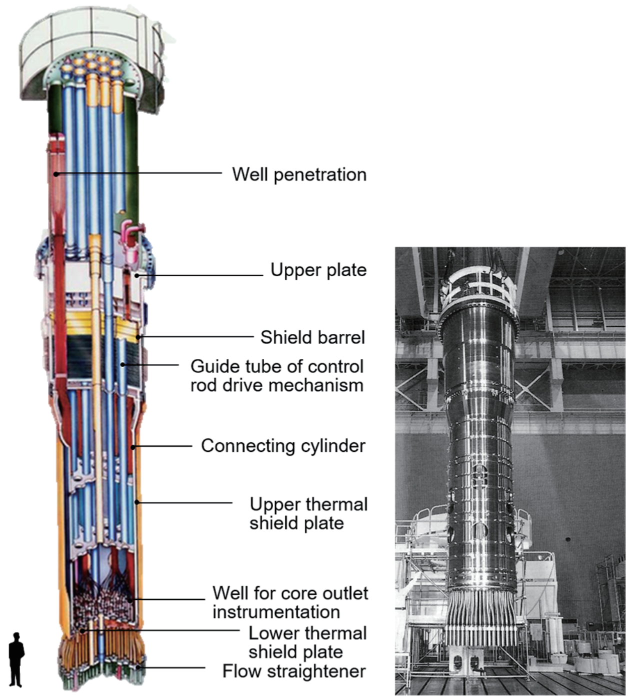

Fig.7-10 Detail of upper core structure

The upper core structure (Fig. 7-10) is installed at the center of the shield plug. It is a top-supported cylinder with a total height of 14 m and a diameter of 2.6 m. The structure supports and guides the CRDMs and the instrumentation wells and consists of the upper plate, shield shell, middle shell, flow guide device, CRDM guide tubes, instrumentation wells, etc.

(1) Design features of shield plug

a) Boundary function for reactor cover gas

Since the PHTS piping was installed at high elevation, the cover gas pressure was set at the slightly high level of 5,500±500 mmAq (54 ± 5 kPa) to prevent the generation of negative pressure during reactor operation. The boundary of the reactor cover gas at the fixed and rotating plugs was sealed by low-melting-point alloy (freeze seal metal with a melting point of 125°C) with backup inflatable tube seal (elastomer seal). The freeze seal metal was developed to have required performances, such as resistance to oxidization, prevention of segregation upon solidification, and good wettability on and adherability with a structural surface. The freeze seal metal is kept in a solidified state when the rotating plug is not operated, such as during reactor operation. When operation of the rotating plug is required, the freeze seal metal is melted to allow the plug rotation, still maintaining the sealing function.

b) Functions to shield radiation and heat from reactor core

A laminated thin-plate structure consisting of stainless steel, carbon steel, polyethylene, etc. was adopted for the fixed plug to shield radiation from the core (Fig. 7-11). In addition, to decrease radiation streaming, a stepped (offset) structure was adopted for the gap between the fixed and rotating plugs, the penetrations of the installed components, etc.

As for the thermal shield function, it is required to minimize heat radiation to above the RV and maintain the temperature of the upper surface of the shield plug at 70°C or less. Thus, a structure with multiple thin stainless steel plates was adopted taking advantage of the thermal insulation effect of gas layers. A cooling layer is provided as well for forced circulation of

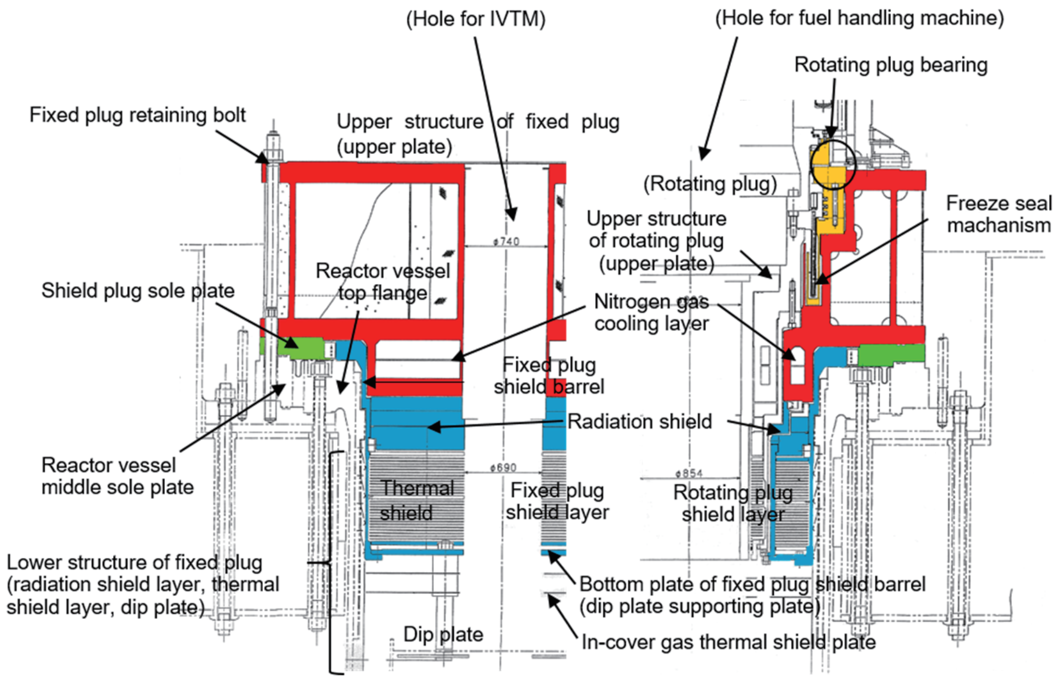

Fig.7-11 Structure of shield plug

nitrogen gas. The pitch between the multi-layered plates was optimized in consideration of the fact that a thicker gas layer would decrease the thermal insulation effect owing to occurrence of natural convection, while a thinner gas layer would negate the thermal insulation effect owing to the bridges formed by sodium vapor deposition.

c) Component installation function

The shield plug has a large-diameter flat plate structure and must support its tare weight and installed heavy components, such as the upper core structure, fuel handling machine, and IVTM. To ensure structural strength and seismic rigidity, a box-shaped structure was adopted for the fixed plug and a thick-plate structure for the rotating plug upper plates.

d) Rotating function for refueling

A single rotating plug with a fixed offset arm was adopted for the refueling method. In this method, the fuel handling device of the fuel handling machine can move to any location in the core, core rack, or IVTM by rotating the plug and fuel handling machine. The rotation plug was developed considering the prevention of deformation during rotation, good positioning accuracy, and minimization of eccentricity during rotation.

e) Measures against thermal striping in the upper core structure

The coolant temperature difference at the outlets of core fuel subassemblies and control rod assemblies would become as large as 160°C. This may induce temperature fluctuation, a phenomenon called “thermal striping”. As a result, high-cycle thermal stress is generated at the near-surface of the upper core structure located above the core. Therefore, an armor structure was adopted in which the components made of SUS304, including the tube plate of the flow guide device and the control rod upper guide tube, are covered by Alloy 718 having excellent high-cycle fatigue strength.

(2) R&D for shield plug

The thermal insulation performance of the shield plug, RV, and the pedestal was confirmed by thermal insulation performance tests, using a mockup device with an actual axial size and a scale of 1/2.5 in the radial direction. In a thermal insulation test to investigate the behavior of the RV cover gas, circumferential temperature non-uniformity was observed in the narrow annulus region of the shield plug, which may cause unfavorable structure deformation. This was caused by the natural convection of cover gas in the annulus. To mitigate this, convection suppressing fins were inserted to the annulus region. Furthermore, various thermal hydraulic tests using water and sodium were performed for a detailed understanding and evaluation of thermal striping phenomenon, and the results were reflected to the design measures for the lower part of the upper core structure.

(3) Manufacturing and installation of shield plug

High accuracies are required for the manufacture, assembly, and installation of the shield plug to ensure the performance of the fuel handling system and the insertability of control rods during earthquake.

As for installation accuracy, the misalignment between the bottom end of control rod upper guide tube (in the upper core structure) and the control rod guide tube at the upper core support plate level was a maximum of 2.51 mm. Even if the error of stop position of the rotating plug and a possible shift during jack-up and down are taken into account, this misalignment does not exceed 5.51 mm; and this satisfies the target value of the integrated manufacturing and installation accuracy. Concerning the levelness, the tilt of the upper plate surface of the fixed plug, the largest component, was confirmed to be 0.03 mm/m, almost perfectly horizontal and satisfied the target value (0.12 mm/m) (Photos 7-3 and 7-4).

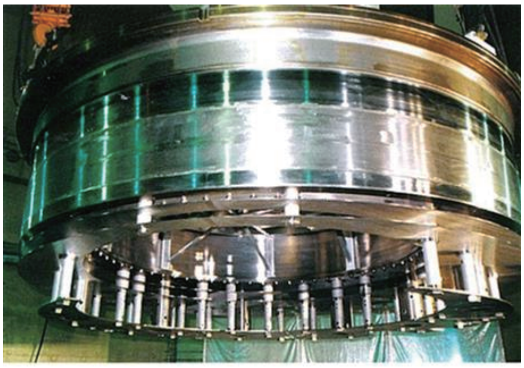

Photo 7-3 Installation of shield plug

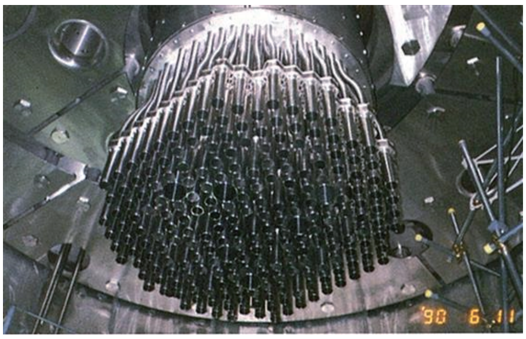

Photo 7-4 View of upper core structure from below

(4) Design validation based on SST

Neutron and gamma dose rates in the pit room above the reactor were measured at a reactor thermal power of 39% and the results were below the lower detection limit, confirming the radiation shielding performance and the effectiveness of the measure against neutron streaming by adopting offset structure in the gap of the shield plug and in component penetrations.

7.2.3 Control rod drive mechanism

The CRDMs are incorporated and installed in the upper core structure and have the following functions: to drive control rod insertion/withdrawal during normal operation, emergency scram, and to delatch control rods during refueling.

The reactor startup, shutdown, and power operations are controlled using the FCRs and CCRs, and the reactor emergency shutdown is performed by the main shutdown system (FCRs and CCRs) and the backup shutdown system (BCRs) activated by a signal from the plant protection system. Major specifications and a structural concept of the CRDM of each shutdown system are shown in Table 7-3 and Fig. 7-12.

The main and backup shutdown systems are mutually independent, including the plant protection systems, and different in the mechanisms to accelerate and disconnect the control rods during a scram (the manufacturers were different as well) to ensure the diversity. Each control rod has an independent CRDM as well: 3 CDRM units for FCRs, 10 for CCRs and 6 for BCRs. The CRDM is comprised of the driving part, upper guide tube, extension tube, etc. and the sealing is formed against the RV cover gas by the bellows in the upper guide tube.

(1) Design features of the CRDM

The design and trial manufacture of the CRDM were conducted efficiently in phases by reflecting the results of early mockup manufacturing and testing to the design of a later mockup.

The bellows of FCRD and CCRD must extend over a long stroke of 1100 mm within 1 s in case of scram, and thus a series of elementary tests were conducted to improve the welding process and the connection structure between flange and end parts of the bellows. Furthermore, since sliding parts are immersed in high-temperature sodium for a long time, surface hardening was applied using Stellite and Alloy 718 to prevent self-welding and sticking of the removable parts, and seizing and galling of the sliding parts.

7. Systems and Components

Table 7-3 Major specifications of Monju CRDM

	Main shutdown system		Backup shutdown system
	FCRD	CCRD	BCRD
(1) Function	· Power control (auto/manual) · Reactor trip	· Power control · Burnup compensation · Reactor trip	· Reactor trip
(2) Number	3	10	6
(3) Driving method	· In normal operation: Ball screw type · In reactor trip: Gravity-driven, gas acceleration type		· In normal operation: Ball screw type · In reactor trip: Gravity-driven, spring acceleration type
(4) Driving speed of manual operation	· 12 cm/min · 3–30 cm/min	· 12 cm/min	· 18 cm/min
(5) Insertion time (on scram)	1.2 s or less (to the 85% insertion from the opening of trip circuit breaker)		
(6) Length (upper guide tube – finger rod)	9,799 mm	9,879 mm	10,000 mm
(7) Main materials	SUS304, SUS304TP (Upper guide tube)		Bored hot-worked stainless bar steel (JISG4003)
(8) Long stroke bellows	· Welded bellows · In low-temperature Ar gas · High-speed expansion	· Welded bellows · In high-temperature sodium · High-speed expansion	· Welded bellows · In high-temperature Ar gas · Low-speed expansion

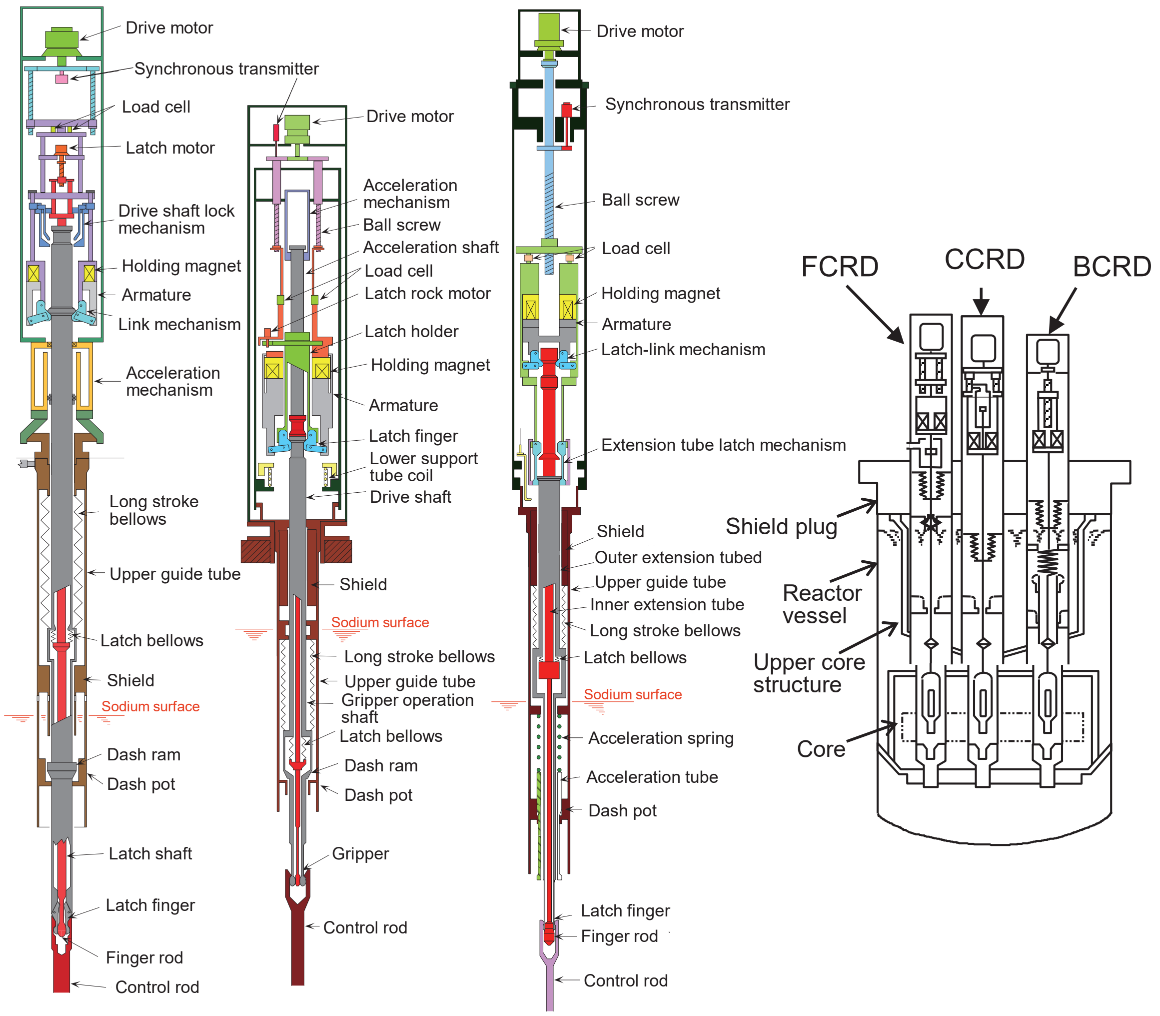

Fine control rod drive mechanism (FCRD)

Coarse control rod drive mechanism (CCRD)

Backup control rod drive mechanism (BCRD)

Fig.7-12 Control rod drive mechanisms

(2) R&D for CRDM

The CRDM is an active component having the crucial functions of reactivity control during reactor operation and emergency reactor shutdown in abnormal conditions. To ensure the reliability of these functions, a significant R&D effort has been made using the prototypes (trial manufacturing) from the early design stage.

The trial manufacture of the mockup was performed in three phases. In each phase, tests were conducted to check various performances, such as:

- The under-water functioning, under-sodium functioning, under-sodium durability for three times the number of activations assumed during the service period of 30 years, and
- Under-water vibration performance (the general performance, structural integrity, and scram performance during earthquake).

Scram tests were performed more than 16,200 times using the prototype, and no failure of control rod insertion occurred. In the under-sodium durability test, intermittent CRDM operation in high-temperature sodium after long-term shutdown was simulated to confirm the presence or absence of self-welding, sticking, and galling of movable parts, the presence or absence of sodium sticking on the interface with the cover gas, and the integrity of bellows. The obtained results were reflected in design and fabrication of the actual Monju CRDM, and accumulated as reliability data for licensing.

(3) Design validation based on SST

In SST, the control rod latch/delatch test, normal drive test, scram performance test, and a test to confirm elongation of the drive shaft were performed for each of the three CRDM types under the condition that sodium was charged and a dummy core was configured in the RV. Regarding the safety-related scram function of the CRDM, a test performed at the rated coolant flow rate confirmed that control rods can be inserted into the core within the specified scram time (1.2 seconds) (Fig. 7-13)[7-2].

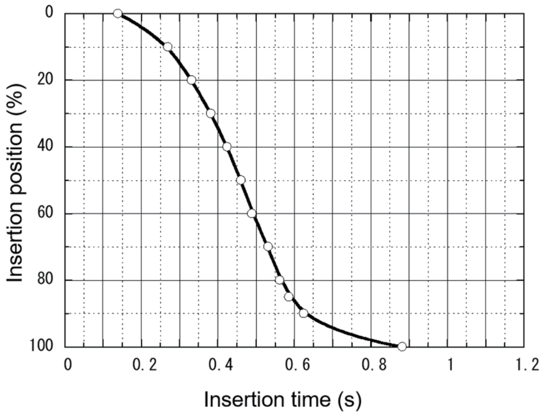

Fig.7-13 Emergency insertion of control rod

7.3 Cooling systems

A system diagram of the Monju cooling systems is shown in Fig. 7-14.

The PHTS consists of three independent loops, each consisting of an IHX, PHTS circulation pump and its overflow column, piping, valves, etc. The PHTS piping is routed at high elevations, and the guard vessels are provided for the IHX and PHTS circulation pump, with the main piping routed at low elevations to connect these components. This arrangement would ensure a sodium level in the RV required

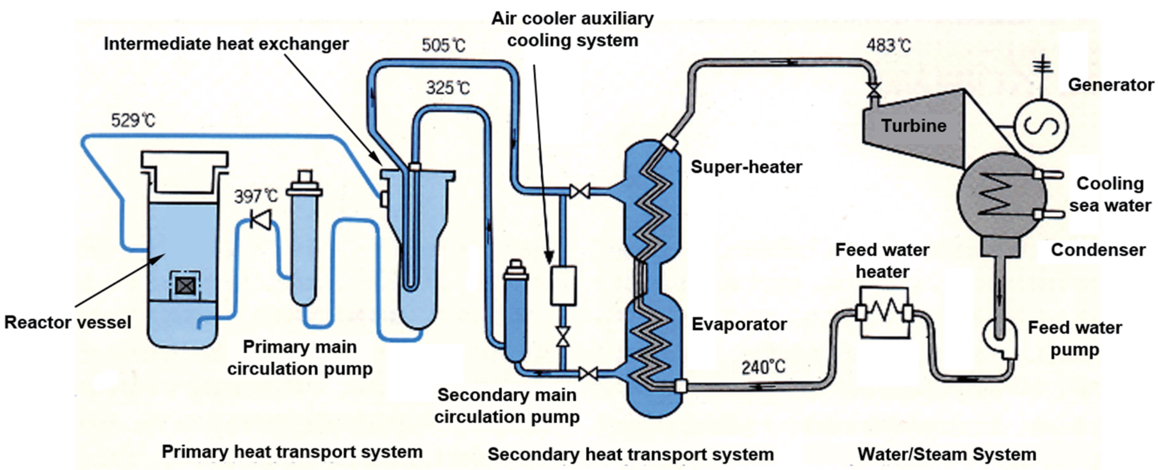

Fig.7-14 Coolant systems of Monju

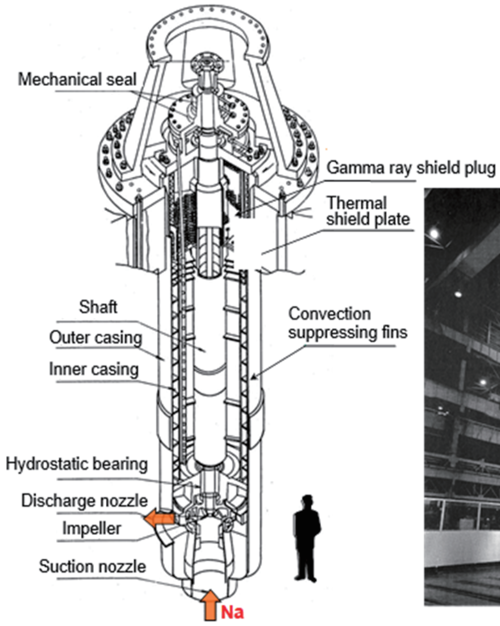

Fig.7-15 Primary main circulation pump

Table 7-4 Major specifications of primary main circulation pump

Item		Specifications
Type		Vertically-mounted free-surface mechanical centrifugal pump
Capacity		~100 m³/min
Head		~92 mNa
Rated rotation rate		~840 rpm
Operating temperature		~400℃
Size	Shell outer diameter	~1.8 m
	Total height	~10.5 m
Main material		Austenitic stainless steel (SUS304)
Number of units		3

for core cooling in case of sodium leak from the PHTS piping.

The SHTS consists of three independent loops, each consisting of the SG (evaporator and superheater), SHTS circulation pump and its overflow column, auxiliary cooling system, piping, and valves. The auxiliary cooling system removes decay heat from the core after reactor trip and during long-term reactor shutdown, such as refueling.

7.3.1 PHTS circulation pump[7-3)]

The PHTS circulation pump (main circulation pump) is a safety-related active component designed to supply a required coolant flow rate to remove heat generated in the core, decay heat, and other residual heat, during normal operation, anticipated operational occurrences, and accidents. The general structure and the major specifications of the main circulation pump are shown in Fig. 7-15 and Table 7-4, respectively.

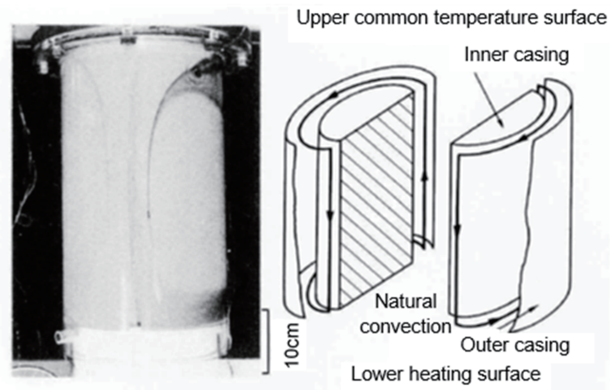

Fig.7-16 Natural convection in the gap between casings

The pump body has a shell diameter of 1.75 m and a height of about 10 m (including the upper shaft seal). Coolant circulation is driven by the main motor (2,000 kW) during the rated power operation and by the pony motor (22 kW) during decay heat removal operation after reactor shutdown. The circulating flow rate can be controlled between 48.6% and 100% by the main circulation pump MG set (variable frequency power supply system of motor generator) to maintain the RV inlet/outlet temperature difference almost constant, regardless of reactor power.

(1) Design features of the main circulation pump

The main circulation pump consists of a pump body and outer casing, and has a structure allowing the extraction of the pump body from the outer casing welded to the PHTS piping for easier maintenance.

In the cover gas space above the sodium surface in the pump, vertical natural convection appears in the gap between the inner and outer casings (Fig. 7-16). This causes a circumferential temperature gradient, leading to thermal deformation of the casing, and may generate excessive load on the pump drive shaft. To prevent this, natural convection suppressing fins (rectangular baffle plate) were installed in the biological and thermal shields. In addition, umbrella-like natural convection suppressing fins were provided in the shaft to prevent shaft bending due to convection of encapsulated argon gas.

(2) R&D for circulation pump

The main circulation pump is the only rotating component that directly handles high-temperature radioactive sodium. Thus, R&D activities on the pump were conducted step by step aiming at high reliability. A scale-up history of circulation pump development is shown in Fig. 7-17. A prototype pump, the first domestically developed unit (capacity of 1 m^3/min) was manufactured in 1966 and was followed by the design, manufacture, and testing of a sodium pump (5 m^3/min), a mockup of the main circulation pump (21 m^3/min). The main Joyo circulation pump for Joy was then developed. The R&D activities for the main Monju circulation pump, which is about five times as large as that of Joyo, focused on development of the shaft bearing and seal, and a full-scale mockup test. The test results were reflected in the design and manufacturing of the actual Monju pump as shown in Fig. 7-18.

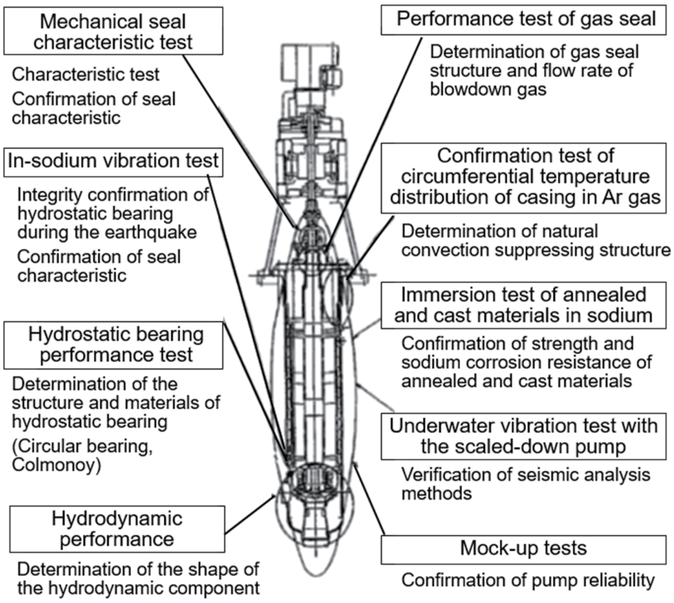

Fig.7-18 Improvement of main circulation pump

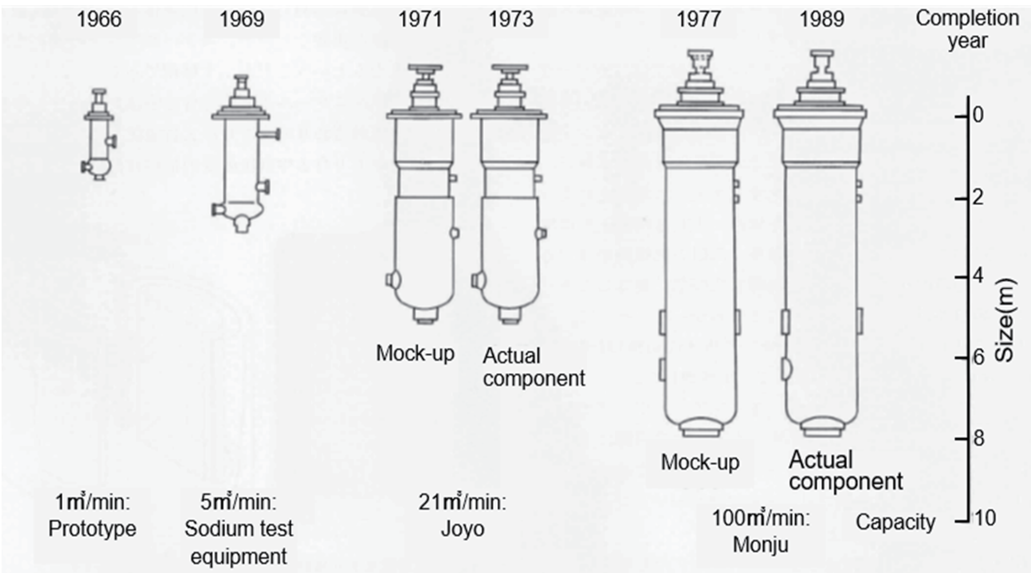

Fig.7-17 Development history of sodium pump for FRs

a) Development of the shaft bearing and seal

Mockup parts tests for the shaft bearing were conducted to obtain design data extrapolatable to actual components. These included tests in water and in sodium and low-speed test, which is more severe for the bearings. For the surface hardener, Colmonoy alloy (Ni-Cr alloy with addition of boron and carbon) having a low cobalt content, a source of radioactive corrosion product, was adopted to reduce radiation exposure.

Double mechanical seals were employed in the pump shaft (Fig. 7-19) to seal the argon cover gas in the pump. The space between the two seals are filled with high-pressure lubricating oil to prevent the leak of radioactive cover gas to the outside. Furthermore, an argon gas diffusion seal is also used, by which the cover gas is purged and shaft sticking due to the deposition of sodium vapor is effectively prevented. Since the operating conditions become more severe with increased shaft diameter, a series of parts tests were performed using a test component of an actual size. Particularly for the argon gas diffusion seal, the effects of the flow rate and pressure of purge gas were investigated in detail and were reflected in the actual component design.

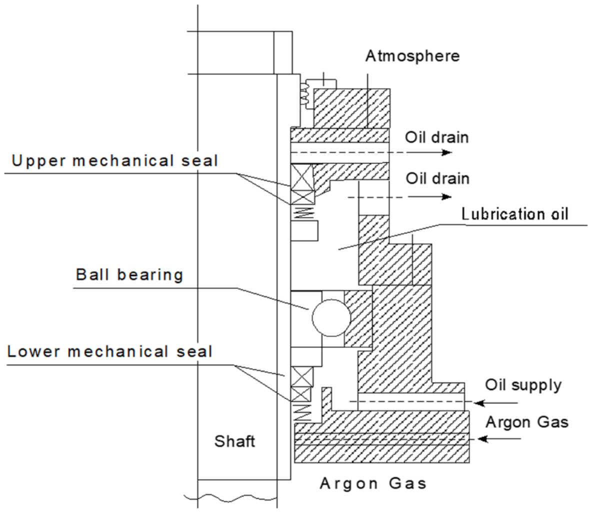

Fig.7-19 Sealing mechanism in the upper part of main circulation pump

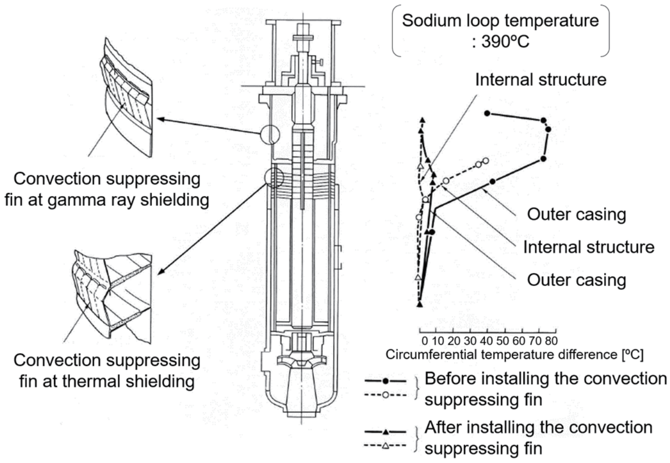

Fig.7-20 Distribution of circumferential temperaure difference measured in mockup pump

b) Full-scale mockup test

In the series of full-scale mockup tests, the pump hydraulic characteristics were confirmed by water tests, and then the mechanical and structural reliability and durability were verified by sodium tests (with a partial flow rate using a special impeller). The main test items and achievements are listed in Table 7-5.

As an example, the axial distribution of the circumferential temperature difference is shown in Fig. 7-20. The effect of the convection suppressing fins installed in the relevant space were found to effectively decrease the peak circumferential temperature difference in the outer casing from 74°C to 10°C, and thereby significantly reduce the amount of thermal deformation of the casing.

Deformation of the casing caused by natural convection in the annulus space became evident in the scale-up from Joyo to Monju. This is a good example showing the importance of sodium mockup tests simulating the actual temperature conditions and the effectiveness of full mockup tests to identify problems due to scale-up. This is also a valuable finding applicable to the design of a reactor component having an annulus space in the cover gas.

(3) Manufacture and installation of circulation pump

The main circulation pump is arranged in the cold leg of PHTS. Its shaft is considerably long (about 8.5 m) because a large liquid surface fluctuation and a gamma shield (about 1.4 m long) are accommodated. Hollow forged steel

Table 7-5 Achievements of mockup pump tests for Monju

Test	Test contents	Achievements	Remarks
Underwater test	Hydraulic performance test Rotation rate: 10%-100% Continuous operation test: 6 h Disassembling investigation	Collection of hydraulic performance data (Q, H, η) Confirmation of no abnormal sliding Confirmation of integrity of each part	-
Under-sodium test	Hydraulic performance test Sodium temperature: 200°C –400°C Low-temperature operation test Sodium temperature: 180°C Startup/stop test Sodium temperature: 200°C, 400°C Stop interval: 0.5–5 h Low-level operation test Sodium temperature: 400°C Level: 100 mm above hydrostatic bearing Disassembling investigation Cumulative operation time: 18,500 h	Confirmed agreement with underwater test results Confirmed circumferential temperature difference and displacement of casing smaller than those in high-temperature sodium Checked bent shaft at shutdown and static torque in restart ↓ Installation of turning equipment Confirmed no problem in circumferential temperature difference and displacement of casing. Confirmation of durability and integrity Confirmation of sodium deposition and sodium cleaning method	In adjustment operation, deformation of casing due to natural convection of cover gas was observed, which caused sticking of hydrostatic bearings ↓ R&D to cope with the issues ↓ Use of convection suppressing fins ↓ Retest and confirmation using mockup ↓ Reflection in the actual component

parts (diameter: 550 mm, thickness: 20 mm) were welded to the shaft at its upper, middle, and lower levels in order to reduce shaft weight and set the resonance rotation speed at a high value. Since high-precision balance is required in the pump shaft, careful attention was paid to shaft bending in the manufacturing process by conducting the shaft runout test under the same high-temperature environment as the operating temperature (about 400°C) after optimization of the supporting base position through automatic measurement of the runout at various levels. In addition, in the manufacturing process, the accuracy of the evenness of the hollow part was strictly controlled to ensure high-precision balance, and thick-walled parts were provided axially at some levels for easy correction of imbalance.

(4) Design validation based on operational data

The main circulation pump has been operated even during reactor shutdown and operational data were accumulated for more than 20 years. Using temperature data from the gas layer in the main circulation pump, the relationship between sodium temperature and the maximum circumferential temperature difference (at the middle level of the gas layer) was investigated (Fig. 7-21). The maximum temperature difference at the upper level in the gas layer was 6°C (design allowance: 10°C), and those at the middle and lower levels in the gas layer were 12°C (design allowance: 15°C). Based on these data, the natural convection suppressing fins proved to be effectively functioning.

7.3.2 Intermediate heat exchanger

The IHX is a “vertically-placed, free surface, straight-parallel countercurrent flow type” heat exchanger designed to transfer heat from the radioactive primary sodium to the non-radioactive secondary sodium. Its structure and main specifications are shown in Fig. 7-22 and Table 7-6, respectively.

The primary sodium at a temperature of 529°C flows into the IHX through the inlet nozzle, rises into the space between the inlet plenum outer shell and the outer shroud, and flows into the heat transfer tube bundle through the inlet windows. In the tube bundle, sodium exchanges heat with the secondary sodium that flows inside the tubes while flowing down between the tubes, and flows out from the outlet nozzle through the outlet windows at a temperature of 397°C. The secondary sodium flows into the IHX from the secondary sodium inlet at a temperature of 325°C, flows down in the downcomer, reverses direction in the lower plenum, rises in the heat transfer tubes while being heated to a temperature of 505°C by the primary sodium flowing outside the tubes, and flows out from the secondary sodium outlet nozzle through the upper plenum.

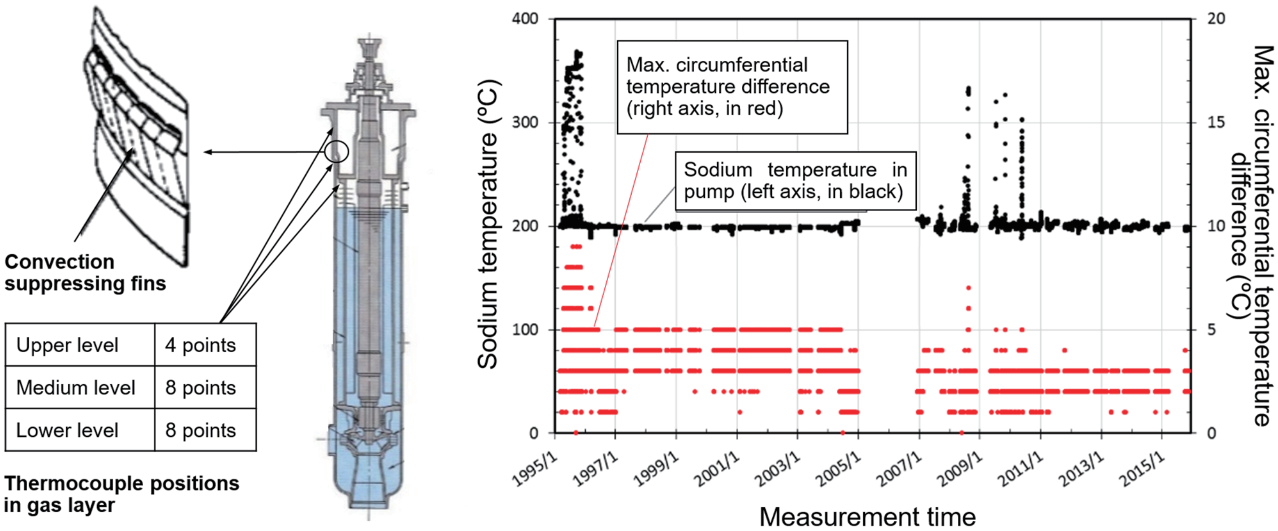

(a) Circumferential measurement points

(b) Measured circumferential temperature differences (at medium level)

Fig.7-21 Maximum circumferential temperature difference and its temperature dependence

Table 7-6 Major specifications of IHX

Type		Free surface, vertically-placed, parallel countercurrent flow type
Number of units		3 (1/loop)
Rated heat quantity transferred		238 MW/unit (2.05 × 10^8 kcal/h/unit)
Rated flow rate	Primary side	5.12 × 10^6 kg/h/unit
	Secondary side	3.74 × 10^6 kg/h/unit
Rated temperature inlet/outlet	Primary side	529°C / 397°C
	Secondary side	325°C / 505°C
Effective heat transfer area		1,093 m^2/unit
Dimension		Shell I.D.: 2.94 m × Height: 12.1 m × Wall thickness: 30 mm
Main materials		SUS304, SUSF304, SUS304TB
Heat transfer tube	Dimension	O.D.: 21.7 mm × Thickness: 1.2 mm
	Number of tubes	3,294
	Array, layers	Circular distribution, 23 layers
	Array pitch	30 mm (radial direction) × 31.4 mm (circumferential direction)

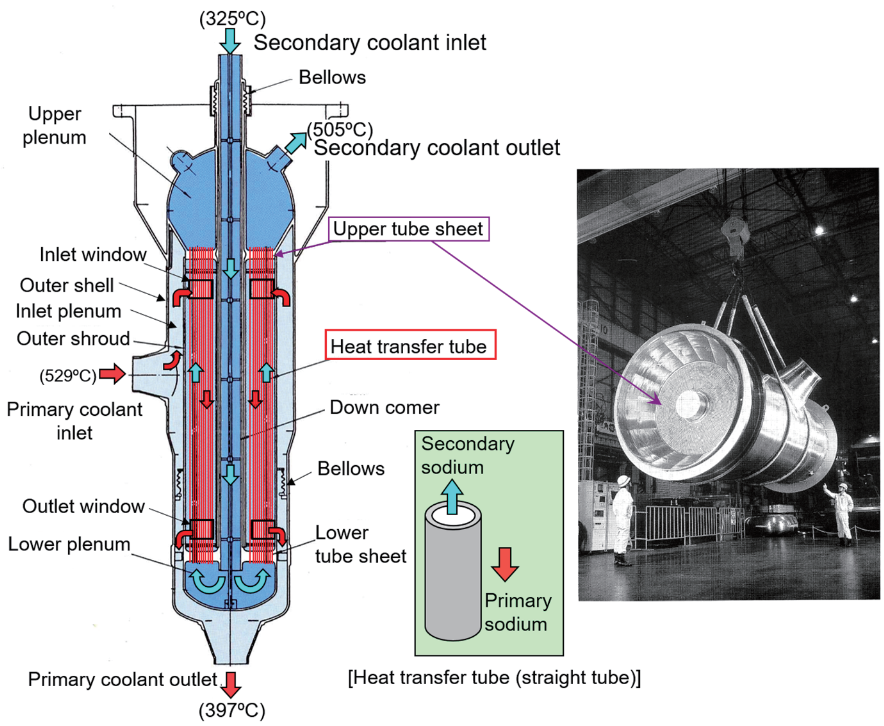

Fig.7-22 Structure of IHX

(1) Design features of IHX

In order to ensure the suction pressure of the main circulation pump, the secondary coolant flows into the tubes with a larger pressure loss, and the primary coolant flows between the tubes and shell. To prevent the radioactive primary sodium from leaking into the SHTS in case of a failure of the IHX heat transfer tube forming the boundary between the PTHS and STHS, the pressure in the IHX primary side was designed to be slightly lower than that in the IHX secondary side.

Since the IHX is operated at temperatures where significant creep occurs and may be used under severe thermal shock conditions caused by high-temperature sodium, sufficient measures were taken to mitigate thermal stress. To prevent component damage due to rapid thermal shock, thermal shield plates were installed at the primary-side inlet nozzle, support skirt, upper and lower tube plates, and secondary-side upper plenum (Fig. 7-23).

(2) R&D for IHX

The IHX of Monju has a heat exchange capacity of 238 MW with a primary-side inlet temperature of 529°C and 3,294 heat transfer tubes. These specifications differ from the IHX for Joyo in the larger heat exchange capacity (about five times), higher operating temperature, and the adoption of a free surface type.

R&D activities were conducted in various fields, including thermal hydraulics, material, structural integrity, and fabrication technologies. Technologies were developed to mitigate thermal stress and to achieve uniform flow distribution in component for high performance.

a) Flow characteristics

Uniform flow distribution is desired to attain good IHX performance and to ensure structural reliability by limiting the temperature difference among heat transfer tubes. Therefore, water flow tests using a full-scale partial model and a small-scale whole model[7-4] were conducted. It was confirmed that uneven flow could be suppressed by adjusting the shape of flow paths in the IHX, the flow guide plates, and baffle shape. Figure 7-24 illustrates the test units used to model the primary-side inlet plenum (half-scale), the heat transfer tube bundle (full-scale, 1/6 sector), and the whole unit (half-scale). Consequently, an almost uniform flow rate distribution was obtained in a full-scale heat transfer tube bundle model, as shown in Fig. 7-25.

b) Material[7-4]

The main material for the IHX, austenitic stainless steel (SUS304), was selected for its superior corrosion resistance and high-temperature strength. For the material used in discontinuous part at high temperatures, the creep rupture strength of SUS304 was increased by limiting carbon and nitrogen to no greater than 0.1%. Concerning the weld material, the contents of trace elements as niobium and vanadium in the base material were optimized by experimentally confirming their effects on high-temperature strength.

c) High-temperature strength and integrity of tube plate[7-5]

Since the IHX is directly connected to the hot-leg piping of the RV outlet, significant thermal shock is applied to the IHX during transients upon reactor trip, PHTS pump trip, and SHTS pump trip. In particular, serious effects are anticipated at the joint between the shrouds and the upper tube plate, on the tube-tube plate joint, and on the primary-side nozzle. A thermal

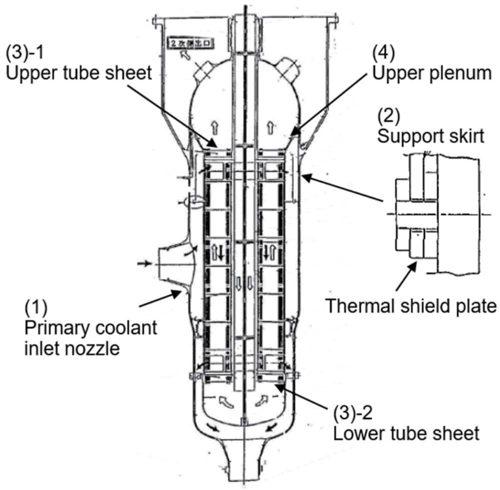

Fig.7-23 Thermal shield installed in IHX

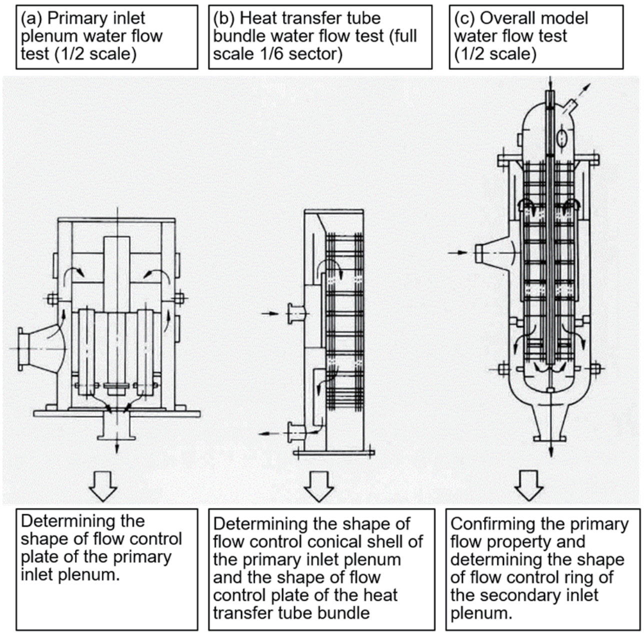

Fig.7-24 Water flow tests to develop IHX

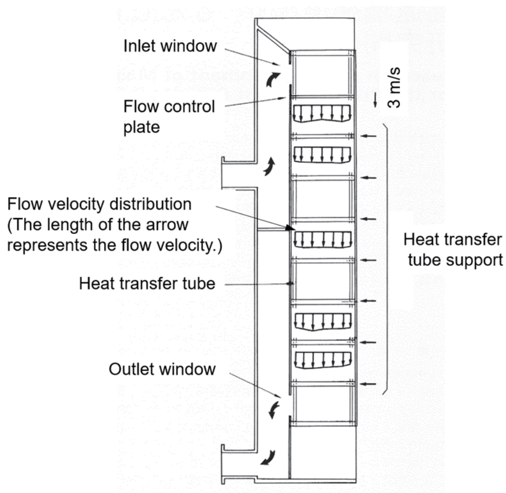

Fig.7-25 Flow rate distribution in IHX heat transfer tubes[7-5]

shock test was performed using a 1/2.5 reduced size test unit to understand thermal hydraulic behaviors at various parts of the IHX.

d) Integrity of heat transfer tubes against compressive buckling

The IHX tube bundle has a configuration in which about 3,000 straight heat transfer tubes are welded at the upper and lower tube plates. When a significant temperature difference between the tubes arises due to nonuniform sodium flow in the tube bundle, compressive load is axially applied to the tubes at relatively higher temperatures, possibly causing buckling. Therefore, a test simulating the actual configuration was conducted to confirm that the strain and horizontal deflection are sufficiently small under the load conditions anticipated in the actual plant.

e) Structural integrity of bellows

Bellows in the IHX are intended to accommodate the thermal expansion difference between the secondary-side downcomer and tube bundle, and between the outer shell and tube bundle. The former bellows forms a part of the reactor coolant boundary. The integrity of these bellows was confirmed through the various tests and stress analysis including fundamental tests for determining the bellows crest, stress measurement, fatigue durability tests, and immersion in sodium.

Table 7-7 Major specifications of Monju SG

Item	Evaporator	Superheater
Type	Integrated once-through helical coil type	Same as left
Number of units	3 (1/loop)	Same as left
Heat exchange capacity	191 MW	47 MW
Heat transfer area	900 m^2	424 m^2
Heat transfer tube		
Number of tubes	140	147
Outer diameter	31.8 mm	31.8mm
Wall thickness	3.8 mm	3.5 mm
Shell		
Outer diameter	~3 m	~3 m
Total height	~15 m	~12 m
Sodium		
Inlet temperature	469°C	505°C
Outlet temperature	325°C	469°C
Flow rate	3.7×10^6 kg/h	3.7×10^6 kg/h
Steam conditions		
Pressure	146 kg/cm^2G	127 kg/cm^2G
Temperature	369°C	487°C
Feedwater (steam) inlet temperature	240°C	367°C
Water-steam flow rate	3.8×10^5 kg/h	3.8×10^5 kg/h
Tube material	2-¼Cr-1Mo steel	SUS321

f) Tube-tube plate welding method

The complete socket welding method was selected for tube-tube plate welding to ensure manufacturability and reliability of the bundled heat transfer tubes. The crevice corrosion, which may occur in a crevice (gap between tube and tube plate), was judged unlikely to occur based on operational experience of sodium components.

(3) Manufacturing and installation of IHX

The IHXs were manufactured in a factory dedicated to stainless steel products with controlled humidity and temperature under a quality control system specialized for Monju based on that for commercialized nuclear reactors. The manufactured IHX thus generally satisfied all required dimensions within the tolerances and was then installed in Monju, so that its lower seismic support fitted the support structure of the guard vessel.

7.3.3 Steam generator

The SG is a component designed to generate high-pressure steam by transferring heat from the heated sodium transported from the core to the SG. Since many troubles were experienced with the SGs of earlier foreign FRs, its performance was considered to be a key to plant availability as well as to plant safety.

To develop the Monju SG, a wide range of R&D activities from fundamental to demonstration tests, were performed to accumulate test data on the thermal hydraulic characteristics, dynamics, stable controllability, and durability, as well as operating records. The achievements were reflected to the design, manufacture, and operation of the actual component of Monju.

(1) Features of SG design

The major specifications of the SG of Monju and its structure are shown in Table 7-7, Fig. 7-26 and Photo 7-5.

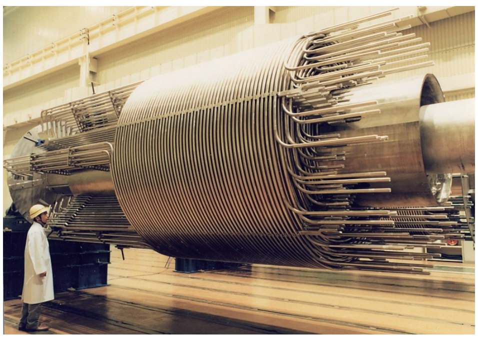

Photo 7-5 Heat transfer tube of SG

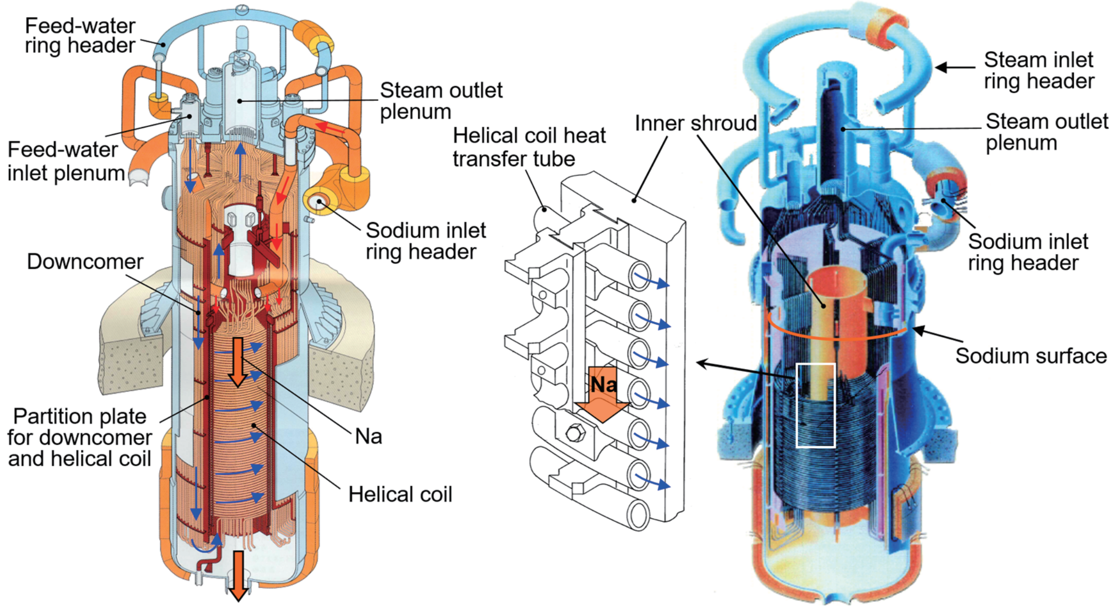

Fig.7-26 Structure of steam generator (left: evaporator, right: superheater)

a) Structural and material features

The SG has the following features:

- A separated type SG consisting of an evaporator (EV) and superheater (SH) was adopted because material satisfying both anti-stress corrosion performance required in the EV and high-temperature strength required in the SH was still in the developmental stage and there was concern about the occurrence of flow instability on the water side.
- As the materials for Monju, a low-alloy steel (2¼Cr-1Mo steel) was selected for the EV in consideration of experience with boilers and anti-stress corrosion performance, while a stainless steel (SUS321 steel) was selected for the SH for its superior high-temperature strength.
- Regarding the type of heat transfer tubes, a helical coil type, which exhibits good heat transfer performance, easily absorbs thermal expansion, and can be compact, was adopted for both the EV and SH.
- Recirculation of steam in the EV was examined in an early design phase because of its advantage in thermal efficiency; however, it was not adopted due to lower reliability and operation controllability with reference to the experience of earlier foreign plants. As a result, a once-through type (non-reheat cycle) SG was adopted.
- The SG has a configuration in which the feed-water inlet/outlet tube plate is above the sodium surface to mitigate the thermal shock at the tube plates and the pressure increase in case of a sodium-water reaction.
- The tube bundle was designed to be suspended from the upper plate or upper shell to allow withdrawal for inspection and repair.

High-temperature sodium (469°C) flows in via the inlet sodium ring header located at the upper part of the EV flows downward between the tubes, and then flows out from the bottom end. Water heated at 240°C flows in via the feed-water ring header located at the upper part, flows downward through the downcomer, is heated while rising in the helically-coiled heat transfer tubes, and then flows out via the steam outlet plenum in the form of superheated steam. The steam is further heated in the SH and then transported to the turbine.

b) Measures against water leak

The SG heat transfer tube is a component that forms the boundary between sodium and water-steam, and hence special attention was paid to ensuring integrity during operation and measures for the failure of a heat transfer tube. The main features are described below.

- No crevice (narrow gap) is provided on the inner (water-steam) side of the tubes to prevent crevice corrosion.
- Hydrogen meters were installed in sodium and cover gas to detect a small-scale water leak.
- To address a large-scale water leak, a pressure relief plate was installed to release excessive pressure. In addition, a reaction product container was installed to suppress

the emission of the reaction products to the air.

- Hydrogen generated in a sodium-water reaction is released and burnt in the air to prevent accumulation in the facility.
- The liner was installed over the inner surface of the shell to suppress wastage-type corrosion in case of a sodium-water reaction.

(2) R&D for SG

Various tests to investigate heat transfer characteristics and reliability were performed using the 1-MW SG test rig, the Instability Test Rig (ITR), and the 50-MW SG test facfility[7-6), 7-7), 7-8)]. An overview of the tests is given below except for R&D activities on the sodium-water reaction described in 4.6.3.

a) Test overview

a-1) Test using 1-MW SG test rig

The 1-MW SG test rig with a heat exchange capacity of 1 MW was constructed with the same structure and specifications of heat transfer tubes as those of the integrated once-through helical coil type SG that was originally planned in the Monju design. A test operation was performed for 6,000 hours from 1971 to 1972 to understand the thermal hydraulic characteristics, structural reliability, and material property change of the heat transfer tube.

a-2) Test using ITR

The ITR was also an integrated once-through helical coil type SG with a heat exchange capacity of 1 MW. It was constructed specifically to clarify the flow instability on the water side. It was also used in a detailed test on dryout and a test to evaluate the dynamic behavior of parameters inside the SG such as temperature distribution on the water side. Taking advantage of the detailed testing capability of the ITR, experimental data on the change in the axial distribution of water-steam temperature were obtained, and the plant dynamics code was validated. Also, data on dynamic characteristics of the state inside the SG were acquired.

a-3) Test using 50-MW SG

Two 50-MW SG test rigs were constructed with the same specifications as those of the separated once-through helical coil type SG finally adopted in Monju (Fig. 7-27).

A test operation of the 1st rig was started in 1973, and a series of tests were carried out on the evaluation of static, water-side flow stability, and dynamic characteristics, as well as on controllability, thermal transient characteristics, and characteristics during accidents focused on the cooling systems. A test operation of the 2nd rig

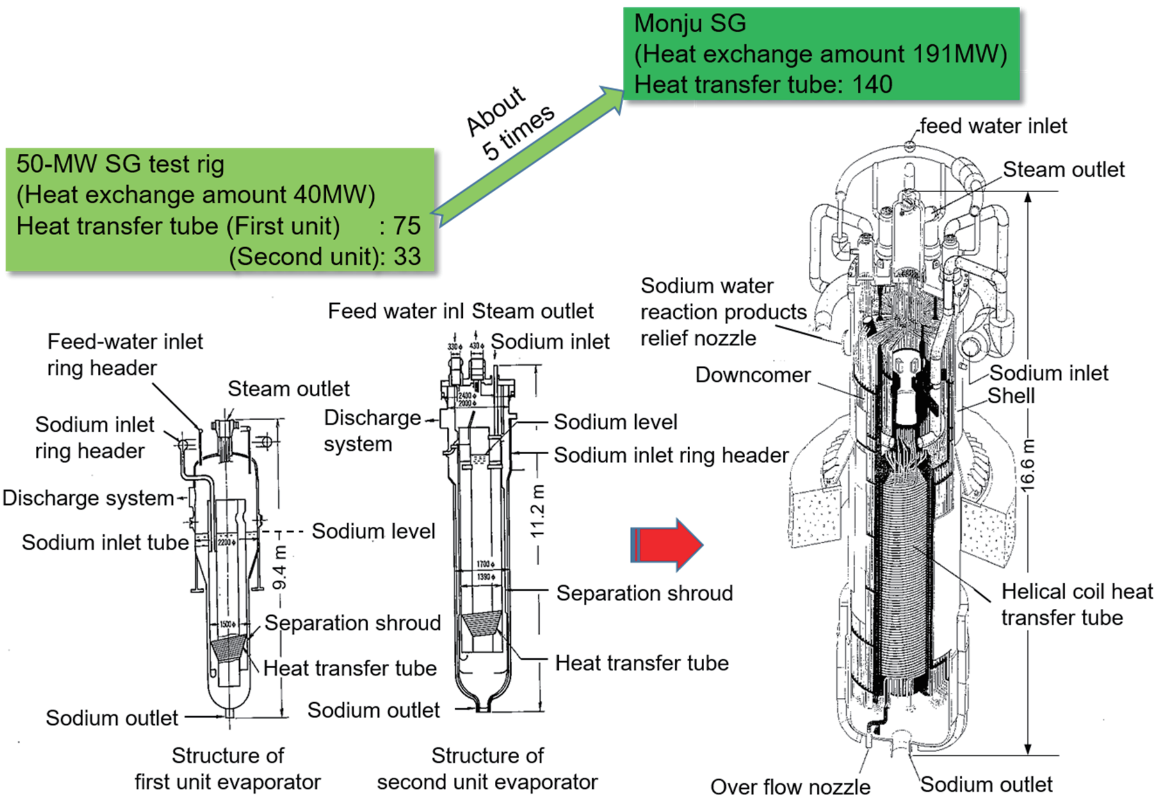

Fig.7-27 Comparison of models between 50-MW SG and Monju

was started in 1976, and a hydrogen behavior evaluation test and a water leak detection test in addition to the same series of tests as performed using the 1st rig were carried out. In 1980, maintenance activities were conducted to demonstrate the withdrawal, cleaning, inspection, and plugging of the heat transfer tubes, and the exchange of the outermost layer of the helical coils.

The total operating hours of rigs 1 and 2 on the water side was 19,500 hours, and that on the sodium side of the SG reached 31,300 hours. During these periods, no failure of a heat transfer tube occurred, demonstrating high performance and reliability of the SG developed in Japan.

b) Development of a thermal hydraulic evaluation formula

Development of a thermal hydraulic evaluation formula was the most basic and important item in the design of the SG. The performance tests using the 1-MW and 50-MW SG were conducted by taking the pressure, temperature, and load level as parameters to evaluate and validate a thermal hydraulic evaluation formulae (for the water-steam-side and the sodium-side heat transfer coefficients), and thereby to establish them as the design formulae for the Monju SG.

c) Measures against water-side flow instability

Water-side flow instability may arise from the fluctuation of the pressure drop of a steam-liquid two-phase flow when the water boils in the heat transfer tubes. An analysis code to evaluate the flow instability of the two-phase flow was developed and validated, and a range of operating conditions that can securely eliminate the occurrence of flow instability has been established as a stability map. This map was used to determine the range of stable operation of the actual component, which was reflected in designing the Monju SG.

d) Understanding of dryout phenomenon in tubes

Water flowing in heat transfer tubes is heated by sodium and boils in a two-phase flow. With an increased ratio of steam (quality) with increased heating, a state in which the transfer tube inner surface becomes dry (dryout state) arises at a certain point. The start of dryout triggers the change in the boiling state from the nucleate to film boiling followed by a rapid decrease in the heat transfer coefficient. Therefore, it is necessary to evaluate with high accuracy the quality to predict heat transfer performance accurately. In addition, the fluctuation of tube wall temperature near the dryout point is important from the perspectives of thermal stress exerted on tubes and thermal fatigue.

To resolve these issues, a test focusing on dryout was performed using a partially modified ITR to clarify the dryout phenomenon in a helical coil type sodium-heated SG. Accordingly, a method to evaluate the dryout quality and thermal fatigue was developed for the design of the Monju SG.

e) Confirmation of material properties and strength

Candidate materials for the SH have good high-temperature strength, but the stress corrosion cracking was a concern. Therefore, several types of austenitic stainless steel were tested under actual plant conditions and accelerated conditions assuming the inflow of wet steam and the increase in dissolved oxygen. Test results confirmed that stress corrosion cracking is unlikely to occur for all tested materials under the assumed operating conditions.

To confirm the aging of material properties, a portion of the heat transfer tubes used at 1-MW and 50-MW SG were cut out for detailed material tests to investigate decarburization and carburization, corrosion on the sodium side, generation of scale on the water side, and the change in material strength. Consequently, no anomaly was found on the heat transfer tube material during extended operation of up to 16,000 hours, and it was confirmed that deterioration due to aging is negligible.

(3) Design and fabrication of the SG

Since many troubles in foreign SGs occurred at heat transfer tube welds, special attention was paid to the welding of the heat transfer tubes. The main points to note are described below.

- Tube to tube plate welding was performed using butt welding, which allows for volume inspection, after machining the tube plate.
- A long tube (EV: about 21.5 m, SH: about 32 m) was adopted for the heat transfer tube to minimize the number of welding zones.
- The heat transfer tubes for the EV are stored in full water containing hydrazine after completion of the water pressure test in factory to suppress corrosion.

7.4 Fuel handling and storage systems

The development of Monju fuel handling and storage systems was based on systems demonstrated in Joyo, and the technology was further enhanced toward FR commercialization. Reduction of the size of the components around the RV was achieved by developing a compact fuel handling machine with a fixed offset arm pantograph refined from the directly driven type used in Joyo. The use of the ex-vessel fuel storage tank (EVST) to eliminate in-vessel storage adopted in Joyo contributed to the employment of a compact RV. The refueling period was minimized using the ex-vessel fuel transfer machine that moves only between the reactor and EVST. The fuel transfer machine was designed to run inside and outside of the CV (Fig. 7-28).

7.4.1 Refueling system

The major specifications and system of the refueling system are shown in Table 7-8 and Fig. 7-29, respectively.

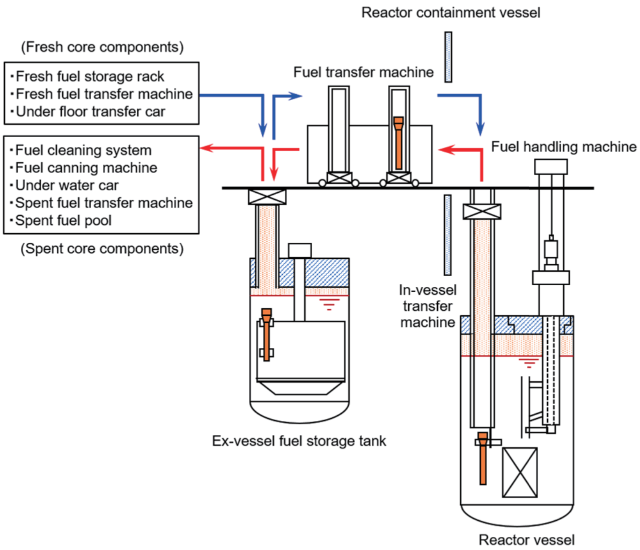

Fig.7-28 Fuel handling and storage systems

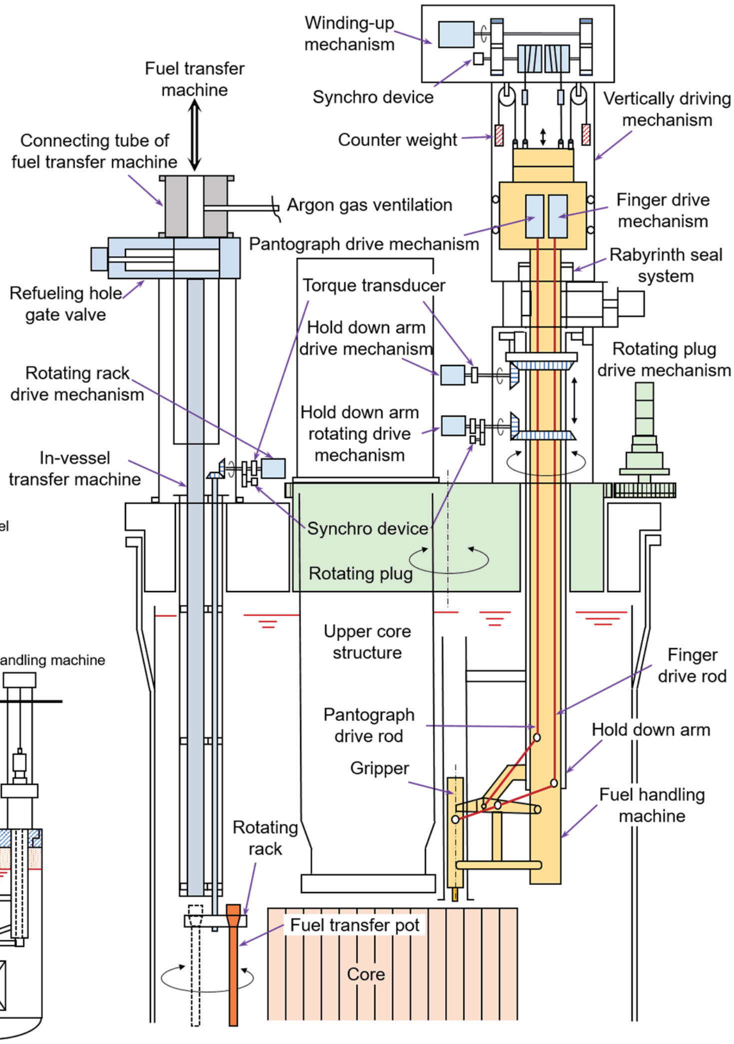

Fig.7-29 Refueling system

Table 7-8 Major specifications of refueling system

	Type	Geometry	Main materials
Fuel handling machine main unit	Pantograph type	Total length: ~14.2 m, Stroke: 4.3–4.6 m	SUS304
Hold down arm and drive mechanism	Fixed offset arm (in-vessel installation)	Total length: ~11.4 m, Arm length: ~1.7 m Up/down stroke: 50 mm (during refueling)	SUS304, carbon steel
IVTM main unit	Rotating rack type	Total length: ~12 m, O. D.: ~0.5 m	SUS304

In refueling, a single rotating plug with a fixed offset arm was adopted in consideration of extrapolation to a larger reactor, reduction of size, plant availability, reliability, ease of operation and maintenance, and safety.

In parallel to the design of the fuel handling machine, mockup tests were conducted in air and in sodium, and it was confirmed that the pantograph type has sufficient capability as the Monju fuel handling machine from the structural, functional, and material aspects, including the positioning accuracy, insertion/withdrawal performance of fuel, decentered operation, self-orientation function, and durability.

7.4.2 Ex-vessel fuel transfer machine

The major specifications and appearance of the ex-vessel fuel transfer machine are shown in Table 7-9 and Photo 7-6, respectively.

(1) Gripper and gripper driving device

A stainless-steel tape type was adopted for the gripper driving device of the transfer machine. The transfer machine consists of the main units A and B, and the general structure of unit A gripper is shown in Fig. 7-30. The main features are described below.

- Since more numerous and larger core elements than Joyo are handled, the appropriateness of the design of the gripper driving device was confirmed by tensile strength and bending strength tests for the tape and winding-up drum considering the lifting load and the operation frequency.
- Two redundant pairs of tape drives were adopted for the gripper driving device to prevent fuel from dropping in case of the failure of one of the drives.
- To reduce the number of fuel transfer components, an adapter-type gripper was devised and demonstrated by testing in sodium. This gripper can handle either fuel transfer pots or core elements that have different handling head shapes.
- In case that the gripping or release of the adapter finger is interrupted, the design enables operation of the gripper finger to handle the core element together with the adapter.

(2) Measures for sodium dripping

The amount of sodium dripping during the handling of core elements is much larger than that of Joyo. Therefore, the following measures were taken:

- The size of the receiver (drip pan) for dripping sodium installed in the door valve was increased.

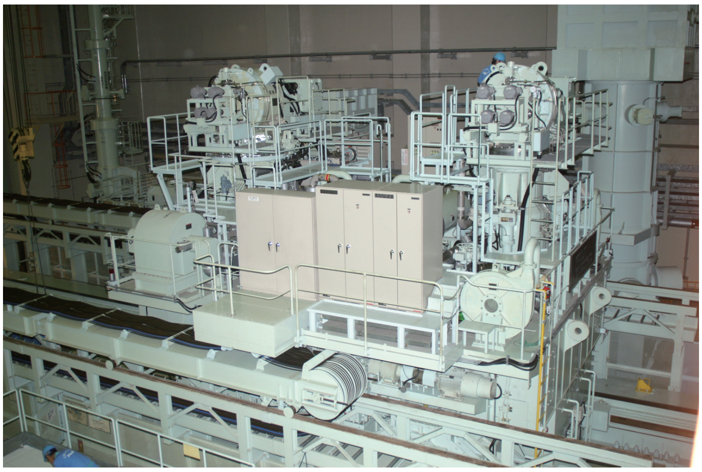

Photo 7-6 Ex-vessel fuel transfer machine

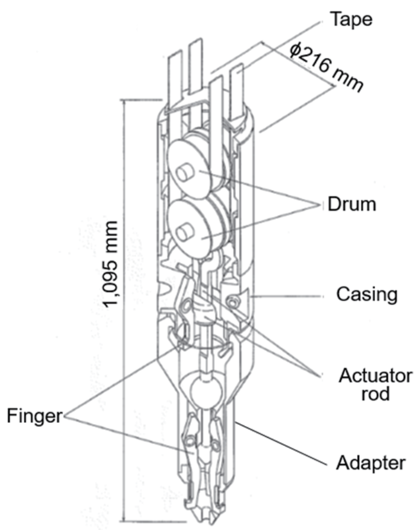

Fig.7-30 Gripper of fuel transfer machine unit A

Table 7-9 Specifications of ex-vessel fuel transfer machine

	Unit A	Unit B
Type	Two pairs of tape drives (detachable adaptor)	Two pairs of tape drives
Objects to be handled	Fuel transfer pot, single core element, drip pan	Single core element, drip pan
Size	O.D.: ~1.2 m × Height: ~8.1 m	O.D.: ~1.1 m × Height: ~8.1 m
Cooling method	Direct/indirect cooling	Direct cooling

- Since the drip pan needs to be replaced periodically during refueling, a drip pan adapter is mounted on the gripper to allow for automatic remote handling in a short time.
- A siphon mechanism is provided for the drip pan to allow for natural discharge of dripped sodium to the EVST.

(3) Ex-vessel fuel transfer machine cooler

The indirect cooling system for ex-vessel fuel transfer machine unit A supplies the cooling air between the walls of a built-in double cylinder to indirectly cool a fuel subassembly. The inner surface of the inner cylinder is coated to ensure the emissivity required for cooling. The emissivity was tested and proved to be ensured even when sodium is deposited on the cylinder.

High airtightness is required for the direct cooling system of ex-vessel fuel transfer machine unit A, which directly cools the fuel subassembly on which sodium is deposited. Thus, a highly air-tight blower was developed, and adaptability was confirmed through prototype tests and integrated tests with the mockup of the ex-vessel fuel transfer machine.

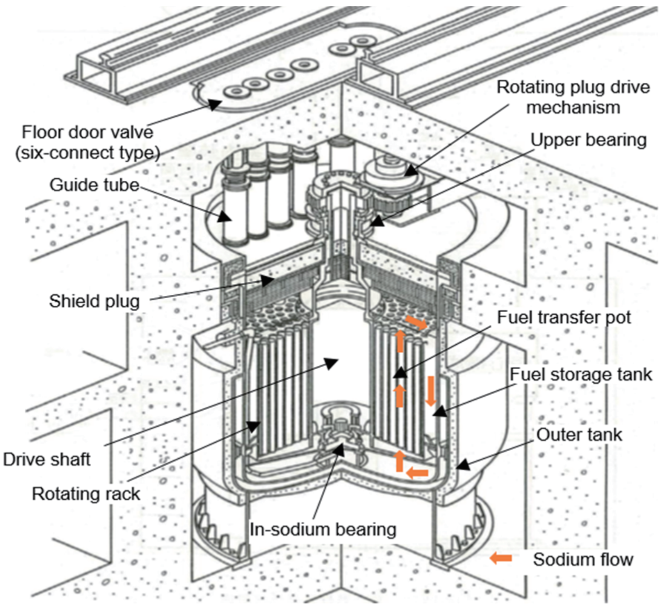

Fig.7-31 Structure of EVST

7.4.3 Ex-vessel fuel storage system

The major specifications of the EVST system are listed in Table 7-10, and the structure of the EVST is shown in Fig. 7-31.

(1) EVST cooling system

The method for cooling the EVST that was first examined was to circulate the primary sodium through the EVST and cool the primary sodium by the secondary cooling system. Subsequently, the primary cooling system was replaced with a direct immersion coil (cooling pipe) for streamlining, which is cooled by the secondary cooling system.

Fuel subassemblies stored in the EVST are cooled by the natural circulation of sodium in the EVST. It is required to circulate sodium both inside and outside of the rotating rack. Therefore, inside the rotating rack, openings are provided as flow paths in the upper, middle, and lower support plates of the rotating rack to allow sodium to rise from the lower to the upper part of the rotating rack. Cooling performance by natural circulation of sodium in the EVST was confirmed using an analysis code validated through water flow tests.

(2) Rotating rack and drive mechanism

The rotating rack of the EVST is too large and heavy to be supported only by the thrust and radial bearings placed on the shield plug of the EVST. Consequently, it was decided to install the in-sodium radial bearing as a stopper of the rotating rack at the bottom of the fuel storage tank.

This bearing should be capable of being

Table 7-10 Major specifications of ex-vessel fuel storage system

	EVST	Rotating rack	Cooling pipe
Type	Fuel storage tank: Vertical cylindrical vessel equipped with bottom end plate Outer vessel: Vertical cylindrical vessel Shield plug: Cylindrical box having beam concrete therein	Storage method: Concentric 6-raw stacked one high Support method: Suspended type	Helical coil type
Size	Fuel storage tank: Shell I.D.: ~6.1 m × Height: ~8.7 m	O.D.: ~2 m × Height: ~4.5 m	O.D.: 88.9 mm × Thickness: 3.2 mm
Main materials	SUS304, SUSF304, carbon steel, concrete	SUS304, SUSF304	SUS304TB
Storage capacity	Fuel transfer pot containing core element: 250 units Empty fuel transfer pot: 1 unit, Drip pan: 1 area (stacked 10 high)		

used in sodium with no lubrication (i.e., lubricated by sodium only) for 30 years and 20,000 cycles of rotation without maintenance and inspection. Thus, the performance was confirmed by testing in sodium. In addition, for replacement in case of bearing failure, a handling head is provided and an access route for replacement is secured by making the rotating rack drive shaft hollow.

(3) Six-series floor door valve

The original design of the floor door valve of the EVST called for the preparation and installation of six units of the proven gate valve-type floor door valves on each row of the rotating rack. However, it turned out to be difficult to install a required amount of shield in the space determined from the storage pitch of the rotating rack. A subsequent design was then proposed and tested in which only one unit moves from row to row, with the consideration of cost saving as well.

However, commissioning proved that the movement would require significant load. Finally, a six-series floor door valve was developed for use in Monju (Fig. 7-32). This door valve adopts a rotary-type valve body to prevent the loss of shielding function.

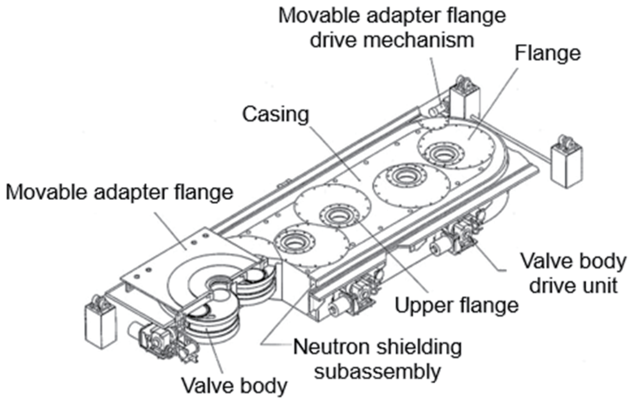

Fig.7-32 Door valve with six-series floor door

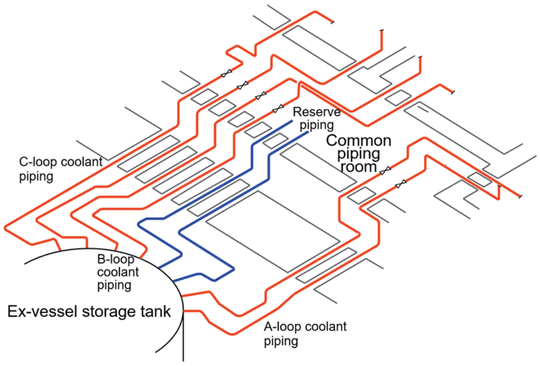

Fig.7-33 Arrangement of coolant piping of EVST

(4) Common piping room filled with nitrogen

The common piping room for the EVST cooling system is used to replace cooling pipe of the failed system with a spare in case of the failure of one of the cooling pipes installed in the EVST. The room initially had an air atmosphere because the temperature increase even in case of sodium leak would be insignificant, causing only minor influence on the other components (piping, valve, etc.) in the room.

In consideration of the Secondary Sodium Leak Accident, however, it was later decided to apply the measures against sodium leak to the EVST cooling system as well. The atmosphere of the common piping room was changed to nitrogen except during maintenance and inspection (Fig. 7-33).

7.4.4 Results of commissioning

An installation test, a single unit functional test, and SKS in air and in sodium were performed for each part of the equipment to confirm the functions and performance of the mechanical, electrical, and control systems. Then, automatic continuous operation tests were conducted to confirm smooth alignment of equipment and sufficient operation monitoring capability including the location management of core elements. It was also confirmed that the handling speed satisfies a condition expected in the system design (refueling operation: 10 subassemblies per 16-hour period, fuel processing/storage operation: 2 subassemblies per 16-hour period).

However, since a rated-power plant operation was not performed, no experience of handling actual spent fuel with large decay heat and radiation dose was accumulated.

7.5 Instrumentation equipment

The Instrumentation equipment was developed with full consideration of the features of sodium cooled FRs. A wide variety of R&D activities were conducted with special emphasis on the reactor instrumentation for neutron detection, and for failed fuel detection and location instrumentation. Almost all Monju instrumentation systems were developed with domestic technologies for future commercialization.

The functions and performance of the developed instrumentation equipment were confirmed through the commissioning tests in Monju.

7.5.1 Neutron instrumentation

The types and functions of the neutron instrumentation are listed in Table 7-11, and its schematic arrangement is shown in Fig. 7-34.

Three neutron flux detectors developed include a proportional counter for a neutron source range monitor (SRM), also covering the fuel loading range, a fission counter for a wide range monitor (WRM), and a gamma-ray compensated ionization chamber for a power range monitor (PRM).

For the SRM, a ^{10}B-coated proportional counter with a sensitivity of 10 cps/nv and a service life of one year was developed in the early design phase. Subsequently, a BF_3 proportional counter was developed for better meeting the required conditions because:

- The SRM is also to be used as a monitoring instrument at the time of an accident.
- The BF_3 proportional counters developed for LWR accident monitoring is applicable to Monju.

The prototype BF_3 proportional counter was developed and successfully tested in the irradiation and durability tests. On the other hand, an irradiation test of the ^{10}B-coated proportional counter revealed the necessity of periodic gain adjustment of the pulse system. Based on these R&D results, it was decided to use BF_3 proportional counters (a neutron detection sensitivity of 30 cps/nv is ensured by combining four counters) as the SRM.

For the WRM, a sensitivity of 0.3 cps/nv is required under high temperature and radiation conditions. A fission chamber was selected, and its durability was confirmed by high-temperature irradiation test under gamma-ray and neutron irradiation environments. Originally a two-channel system covering the intermediate range was planned. However, to ensure the diversity of neutron detectors for reactor trip in an event of abnormal reactivity insertion during power operation, the design was changed to use three channels and add an electric current mode so as to cover the wider range from 10^{-6} to 120% of the reactor power.

Table 7-11 Types and features of neutron instrumentation system

Monitor type	Number of detectors	Measurement range (reactor power)	Detector type	Main functions
SRM	2	10^{-8}% –10^{-3}%	BF_3 proportional counter	・Monitoring of subcriticality during reactor shutdown, accident monitoring instrumentation ・Monitoring of neutron flux level during reactor startup/shutdown
WRM	3	10^{-6}% –120%	Fission counter	・Monitoring of neutron flux level during reactor startup/shutdown, backup for the PRM
PRM	5	1%–120%	Gamma-ray compensated ionization chamber	・Monitoring of the level and change rate of neutron flux ・Signals for the plant protection and instrumentation and control systems

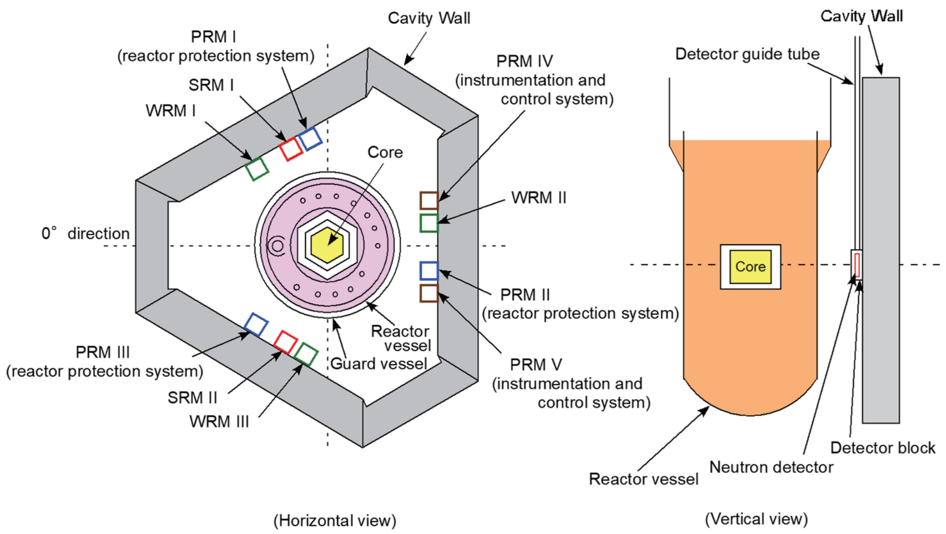

Fig.7-34 Arrangement of neutron detectors

For the PRM to be used under high gamma-ray background (BG), a gamma-ray compensated ionization chamber that can be used at high temperatures was developed. A gamma-ray compensated ionization chamber of voltage compensation type was experimentally developed and its durability was confirmed in Joyo.

7.5.2 Failed fuel detection system

(1) Failed fuel detection system by delayed neutron method

The failed fuel detection system by delayed neutron (DN) method was employed in Monju as one of the plant protection system instrumentations. Locations of the detectors were determined considering delay time due to transport and dilution by mixing of DN precursors released from failed fuel in the RV upper plenum. These effects were confirmed by water flow tests.

The BG count rate of the DN method during normal operation was estimated to be 45 cps in the design considering the photo neutrons from the concrete wall, the neutrons from the core, surface contamination on fuel pins, etc. However, from the results obtained in the 40% power test in 1995, the BG count rate at the rated power operation was estimated to be 1/50 of the design. Consequently, a neutron source (Am-Be) was newly installed at the tip of each DN detector to ensure a meaningful BG count rate (a dozen cps). This improvement was necessary to prevent false alarm and operation check of the DN method system.

The layout of the DN method equipment is shown in Fig. 7-35. A schematic drawing of the improved DN detector (BF_3 proportional counter) is shown in Fig. 7-36.

(2) Failed fuel detection system by cover gas methods

The failed fuel detection systems using cover gas include the precipitator method and the gamma-ray detection method, both of which detect radiation from rare gases (krypton and xenon) released from failed fuel and transported to the cover gas region.

Regarding the precipitator method, "a gas replacement type precipitator" was selected because of higher detection sensitivity, high reliability, and easier maintenance and inspection. A prototype precipitator was produced and improved for Monju, and its performance was confirmed by durability test in the research reactor JRR-3.

Regarding the gamma-ray detection method, an NaI scintillator was installed in the cover gas system, which directly measures the gamma rays emitted from rare gases and is intended to detect a larger-scale fuel failure than that covered by the precipitator method.

During the Core Performance Confirmation Tests in 2010, "the precipitator count rate high" alarm was frequently activated. The cause is presumed to be the flux of fine metal powders produced in a site maintenance work. Subsequently, measures were taken for the removal of foreign materials from the system by gas blow, installation of an argon gas filter to remove foreign material at the detector inlet, and replacement of the three detectors. A certain effect on noise reduction was confirmed, but no reduction of the BG count rate was observed during the test operation after the above measures. The cause of this problem has not been identified.

Regarding the gamma-ray detection method, the results of the 40% power test in 1995 revealed that the BG count rate at the rated power was sufficiently lower than the design value of 340 cps. Consequently, it was

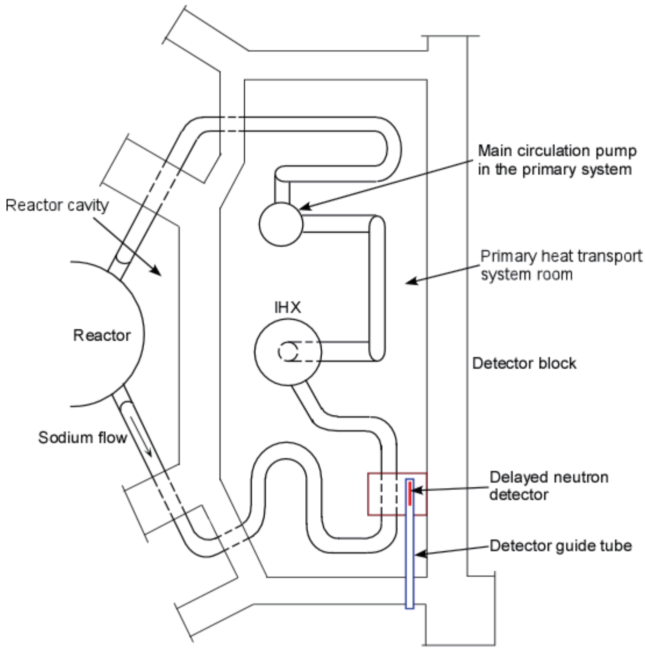

Fig.7-35 Failed fuel detection system by DN method

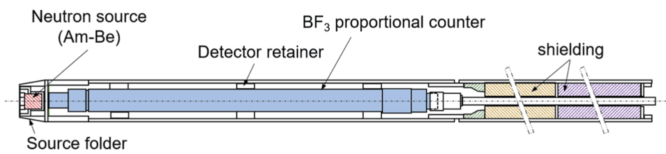

Fig.7-36 Neutron detector of DN method

confirmed that smaller-scale fuel failure, which the precipitator was expected to detect, would be detectable by the gamma-ray detection method as well.

A schematic drawing of the precipitator detector and the overall cover-gas detection system diagram is shown in Figs. 7-37 and 7-38, respectively.

(3) Failed fuel detection system using tagging gas method

Two methods were examined to identify the location of failed fuel: the selector valve and tagging gas methods. In Monju, the tagging gas method (Fig. 7-38) was adopted as the Failed Fuel Detection and Location system, in consideration of the configuration of the upper core structure and experience in foreign FRs.

The tagging gas method identifies the location of failed fuel by detection and analysis of the tag gases encapsulated in each fuel element. Different compositions of stable krypton (Kr) and xenon (Xe) isotopes are assigned to each of the fuel subassemblies. The U.S. and France were leading the development of this method, but there remained certain challenges.

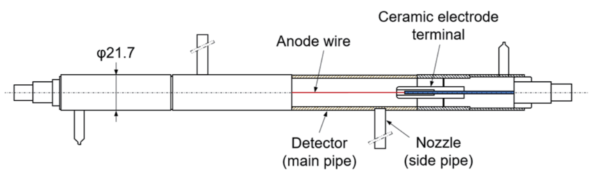

Fig.7-37 Precipitator detector

These included the understanding of gas transport behavior, the development of a compact concentrator/separator, an analysis computer code to model tag gas generation and incineration, and the development of a tag gas capsule.

Concerning the tag gas capsule, a new method using a shape-memory alloy was developed for actual use in the reactor. Concerning the development of the tag gas concentrator/separator, basic data using a small-scale activated charcoal bed were obtained on temperature, time, and carrier gas flow rate in the gas recovery and desorption processes. Based on these data, it was foreseen that nearly 100% of gas could be recovered.

In the Monju design, the recovery time of the tag gas was revised by using a large-scale activated charcoal bed; however, a gas recovery rate of 100% could not be achieved because of a smaller recovery rate for Kr than for Xe. The cause of this small recovery rate was thought to be excessive time required for rare gas desorption due to the fact that temperature was not sufficiently increased in the interior of a large-diameter adsorption bed because of the small thermal conductivity of the activated charcoal. Consequently, a U-shaped adsorption bed with the original smaller outer diameter and twice the previous length was adopted in the actual plant.

Despite the above improvement, the tag gas recovery rate did not reach the specified value

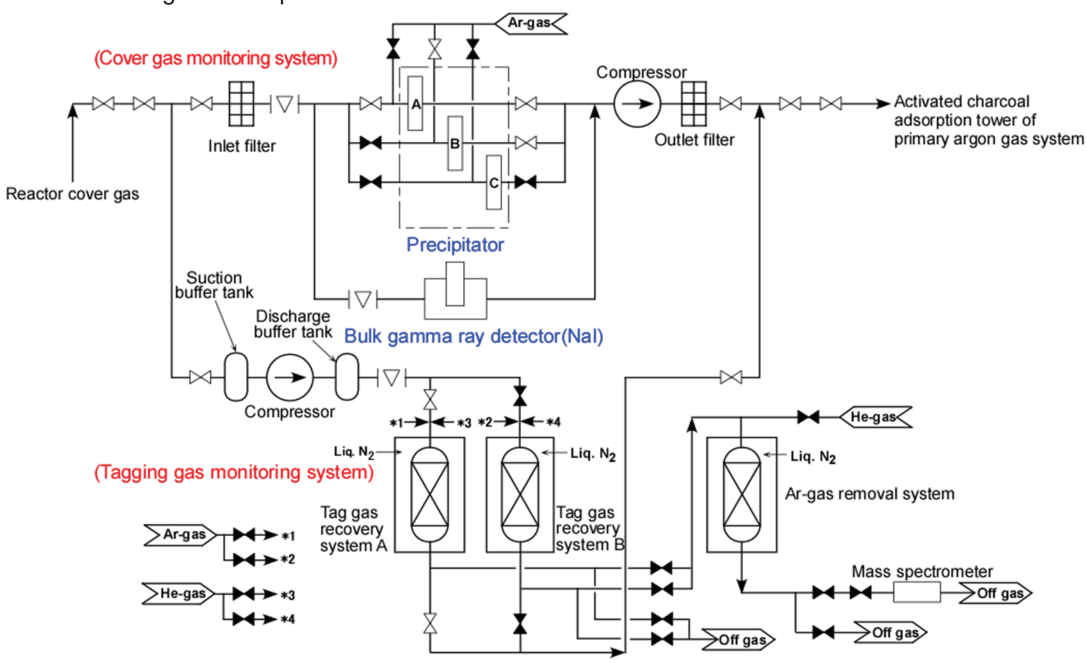

Fig.7-38 Failed fuel detection system using cover gas

(in particular, the recovery rate of Kr was lower by two orders of magnitude) in SKS and SST because the activated charcoal temperature could not be properly controlled.

Consequently, further improvements were attempted by changing the method of introducing the sample gas into mass spectrometer and replacing the liquid nitrogen supply valve with the control valve. The resultant tag gas recovery rate was somewhat improved.

Nevertheless, stable performance has not yet been confirmed. It is necessary to continue a series of confirmation operations and tests to establish a method of controlling the activated charcoal adsorption bed temperature using liquid nitrogen. In addition, because the primary argon gas system has a high BG of rare gas nuclides, the same nuclides as the tag gas, it is necessary to develop a procedure and secure sufficient time to purge the system with fresh argon gas.

7.5.3 Sodium leak detector

The uses and types of sodium leak detectors are listed in Table 7-12. In the development of sodium leak detectors, the focus was placed on a gas sampling type sodium leak detector capable of detecting fine leaks. R&D necessary to demonstrate the feasibility of the gas sampling type as a leak detection system included: the detector itself, the generation and attenuation characteristics of aerosol, self-plugging behavior, corrosion caused by leaked sodium, and a method of gas sampling. From this R&D, it was confirmed that a sodium leak with a rate of 100 g/h can be detected within 24 hours in both the primary and secondary systems. For the leak detectors in the EVST and its cooling system, the amount of aerosol generated is less due to the low system temperature, and it was confirmed that a sodium leak with a rate of 100 g/h can be detected within 150 hours.

The types and principles of fine/small leak detectors are listed in Table 7-13. Based on experience in the commissioning tests, the following improvements were made:

- Platinum filament with a purity of 99.999% is used in the SID to suppress BG increase due to impurities.
- The alarm setting of the RID was originally based on the absolute value of output signal. However, it was revealed that the RID signal depends on the atmospheric temperature (i.e., the output decreases with increasing temperature) and notable signal fluctuation associated with the ionization of ^{241}Am was observed. Accordingly, a digital signal processing system using the moving average method was added.

Table 7-12 Uses and types of sodium leak detectors

Detection target	Fine/small leak from components/piping				Intermediate/large leak from components/piping	
Use	Alarm			Alarm Automatic shutdown of HVAC	CV separation and reactor trip	
Detector	Gas sampling type sodium leak detector SID: Sodium ionization detector DPD: Differential pressure type detector RID: Radiative ionization detector		Contact-type sodium leak detector	Cell monitor in air atmosphere ･Smoke detector ･Heat detector	Sodium level meter (for detecting sodium leak)	Thermometer (for detecting sodium leak)
Location	Major components in primary and secondary systems (RV, pump, IHX), space between piping and heat insulator*1	PHTS room (backup for the above locations)*1	Bottom of tank, near valve bellow seal, under piping	Rooms filled with air where components/piping containing secondary sodium are installed.	In the guard vessel for RV, pumps and IHXs	Primary cooling system room floor
Detection method	Detect (gaseous) sodium aerosol leaking from components/piping*2		Direct detection of sodium leak from components/piping	Detect sodium fire due to leak of secondary sodium to the outside of heat insulator	Detect the level of sodium accumulated in the guard vessel	Detect the temperature of leaking sodium accumulated on the floor
Remarks	*1: Gas sampling point *2: Aiming to detect a leak rate of 100 g/h within 24 hours			Detect fire in the air caused by sodium leak rate of 10 kg/h or more to the outside of heat insulator	Plant protection system	

- Deteriorated insulation or false activation of leak alarm occurred in a silver-soldered closed CLD at high temperatures. The ion migration of silver solder causes the deterioration and short circuit (a phenomenon that causes migration of ionized metal atoms between electrodes, resulting in short circuit). Therefore, a gold-soldered closed CLD in which ion migration is insignificant was introduced.

Table 7-13 Types and principles of sodium leak detectors

<table>
<tr><th colspan="2">Type and principle of detector</th><th>Schematic drawing of detector</th></tr>
<tr><td rowspan="2">Gas sampling type sodium leak detector</td><td>Sodium ionization detector (SID)

Sodium aerosol in sampling gas introduced to detector is dissociated and ionized by filament kept at a high temperature, and the ion current flows between filament collectors. By detecting this ion current, a fine sodium leak can be detected.</td><td>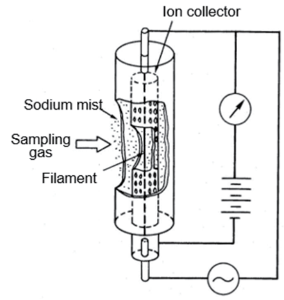
</td></tr>
<tr><td>Radiative ionization detector (RID)

Sodium aerosol in sampling gas introduced to detector adheres to gas ionized by Am-241, decreasing the electric current flowing between electrodes to which external electric field is applied. By detecting this change in electric current with the voltage difference from the reference ion chamber, a fine sodium leak can be detected.</td><td>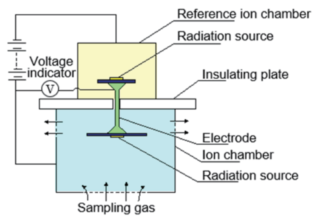
</td></tr>
<tr><td colspan="2">Contact-type sodium leak detector (CLD)

The electric conductivity of sodium is utilized. When leaking sodium adheres between detector electrodes or electrode and the earth, an electric current flows. By detecting this electrical short circuit, a sodium leak is detected.</td><td>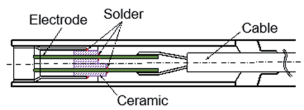

Closed CLD</td></tr>
</table>

— References —

7-1) IAEA, Benchmark Analyses of Sodium Natural Convection in the Upper Plenum of the Monju Reactor Vessel, IAEA-TECDOC-1754, 2014, 180p.

7-2) Hiroi, H. et al., The Test Run of Fast Breeder Prototype Reactor Monju, PNC Technical Review, PNC-TN1340 96-004, 1996, pp.49-68 (in Japanese).

7-3) Yamagishi, Y. et al., Design and Manufacturing of Primary Sodium Pump for the Prototype Fast Breeder Reactor Monju, Hitachi Hyoron, Vol.71, No.10, 1989, pp.23-30 (in Japanese).

7-4) Inoue, T. et al., Design and Fabrication of the Intermediate Heat Exchanger in the Primary Heat Transport System for the Prototype Fast Breeder Reactor Monju, Hitachi Hyoron, Vol.71, No.10, 1989, pp.15-22 (in Japanese).

7-5) Kawahara, M. et al., Research and Development of Main Components for the Prototype Fast Breeder Reactor Monju, Hitachi Hyoron, Vol.64, No.8, 1982, pp.73-78 (in Japanese).

7-6) Takahashi, T., Development of a Sodium-Heated Steam Generators, Journal of the Japan Society of Mechanical Engineers, Vol.81, No.711, 1978, pp.151-156 (in Japanese).

7-7) Tsuchiya, T., Current Status of Steam Generator Development for LMFBRs, Journal of the Atomic Energy Society of Japan, Vol.25, No.5, 1983, pp.320-328 (in Japanese).

7-8) Fukuda, T., Recent Trend of Fast Breeder Reactor Technology Development (3) – Steam Generators for FBR –, Genshiryoku Kogyo, Vol.31, No.1, 1985, pp.64-72 (in Japanese).

8. Sodium Technology

- **Liquid metal sodium used as a coolant of FRs is opaque, chemically active and has a high boiling point. Vast knowledge and technologies were accumulated through R&D on the development, operation, and maintenance of sodium components for safe use in Monju.**
- **The technologies for sodium handling and purity control were established through the operation of various sodium test facilities and the commissioning of Monju.**
- **The technologies of in-service inspection (ISI) have been established through the development of inspection methods and devices applicable under FR-specific conditions. The developed technologies have been successfully applied to the Monju ISI.**
- **In order to reduce radiation exposure to plant workers during maintenance and inspection, cobalt-free materials are used to suppress the generation of radioactive corrosion product. Computer codes were developed to analyze the behavior and removal of radiation sources and to evaluate dose rate distribution.**

8.1 Development of sodium handling technolgies[8-1)]

(1) Sodium purity control technologies

Sodium purity must be appropriately controlled to prevent corrosion of the structural materials of the components and piping, and the fuel cladding. The impurity concentrations in the sodium must be kept low for the reduction of exposure caused by radioactive corrosion products in the PHTS and improved detectability of water leaks from a SG tube in the SHTS. The reduction of impurity, therefore, focuses on oxygen in the PHTS and hydrogen in the SHTS.

Sodium purity is maintained and controlled within a prescribed range using a cold trap (CT) for the removal of impurities in sodium, and a plugging (PL) meter for measuring the impurity concentrations. The CT and PL meters operate on the principle that the solubility of impurities in sodium decreases as the temperature is lowered. Their performance has been confirmed in various sodium test facilities and operating methods have been established. In the initial sodium purification operation, the prevention of blockage is important in low-temperature sections of piping around the CT since a large amount of impurities are attached to the surfaces of as-fabricated components and piping.

(2) Sodium cleaning technologies[8-2)]

Since sodium burns in air and vigorously reacts with water, it is essential to remove the sodium adhering to the components and piping when repairing or modifying the reactor or test facilities. A sodium cleaning method is selected considering factors, such as the size and shape of the object to be cleaned, the amount of sodium adhering to the surface of the components and piping, the presence or absence of radioactive sodium, inspection after sodium cleaning, and reusability. The sodium cleaning methods are divided into physical and chemical methods. The former, including scraping, cannot remove sodium completely, and is thus generally employed in a preparatory step before a chemical method (Fig. 8-1). For the latter, past cleaning experience includes:

- Water cleaning (cold water, hot water and hot-water decompression boiling cleaning)

  This method is used in the finishing step since it is effective for cleaning small amounts of sodium on complex shapes and in crevices.

Fig.8-1 Sodium cleaning tools (physical method)

- Steam cleaning (in air, in an inert atmosphere or using a mixture with inert gas)

  Compared to water cleaning, the reaction with sodium is milder. This method is capable of completely removing sodium and is frequently used. However, attention must be paid to corrosion caused by cleaning liquid waste.

- Alcohol cleaning

  As the reaction of alcohol with sodium is extremely mild, this method is used when cleaning an object for use in a material test. Attention must be paid to preventing the alcohol from catching fire.

- Carbon dioxide treatment

  This method is applicable to components with large and complex structures. Carbon dioxide stabilizes sodium by forming sodium carbonate and was used to clean a tube bundle of the 50-MW SG used in a mockup test.

(3) Development of sodium extinguisher

In handling sodium, protection against fire (and fire extinction) is essential. Sodium is classified as a type 3 hazardous substance under the Fire Service Act. According to the Act, dry sand can be used as an extinguisher, but it should be stored in a dry state. In addition, dry sand is not suitable for a large-scale sodium fire since a suffocation effect may not be expected because it is heavier than sodium. Therefore, an extinguisher consisting mainly of anhydrous sodium carbonate powder (product name: NATREX) was developed in collaboration with a fire extinguisher manufacturer. Performance of the extinguisher was tested at the National Research Institute of Fire and Disaster, and was approved as an extinguisher for sodium fires. The NATREX extinguishers are installed in the sodium test facilities, Joyo, and Monju (Photo 8-1).

Photo 8-1 NATREX fire extinguishers

8.2 Development of sodium components

(1) Cold trap

The CT is a device designed to purify sodium. It supersaturates and precipitates oxygen and hydrogen in sodium by lowering the sodium temperature (generally to 120°C–150°C) and traps the precipitates with a stainless steel mesh. It is usually installed in a purification system branching from main sodium circulation systems. When the CT is in continuous use over an extended period, the mesh part becomes clogged with impurities. Thus, uniform trapping of the impurities in the mesh was a major R&D issue.

Through various tests in the sodium test facilities of the OEC and operating experience in Joyo, findings were obtained on a flattened temperature distribution in the CTs, an increase in the inflow areas of the mesh parts to prevent local blockage formation, and optimization of the mesh packing density. The findings were reflected in the Monju CT design (Fig. 8-2).

CTs in the secondary cooling system are subjected to a heavy load caused by impurities due to the permeation of hydrogen from SG tubes during plant operation, and thus need to be replaced during the plant lifetime. For this reason, R&D activities on the regeneration of the CTs were conducted to reduce waste, and the applicability to an actual plant was examined.

(2) Plugging meter

The PL meter is a simple instrument designed to continuously measure impurities in sodium. The measurement principle uses the precipitation of an impurity in sodium at a temperature equal to or lower than its saturation temperature. The impurity concentration in sodium is estimated based on the relationship between a measured saturation temperature and the saturated solubility of the impurity. A large number of PL meters have been successfully used in the sodium test facilities of the OEC and

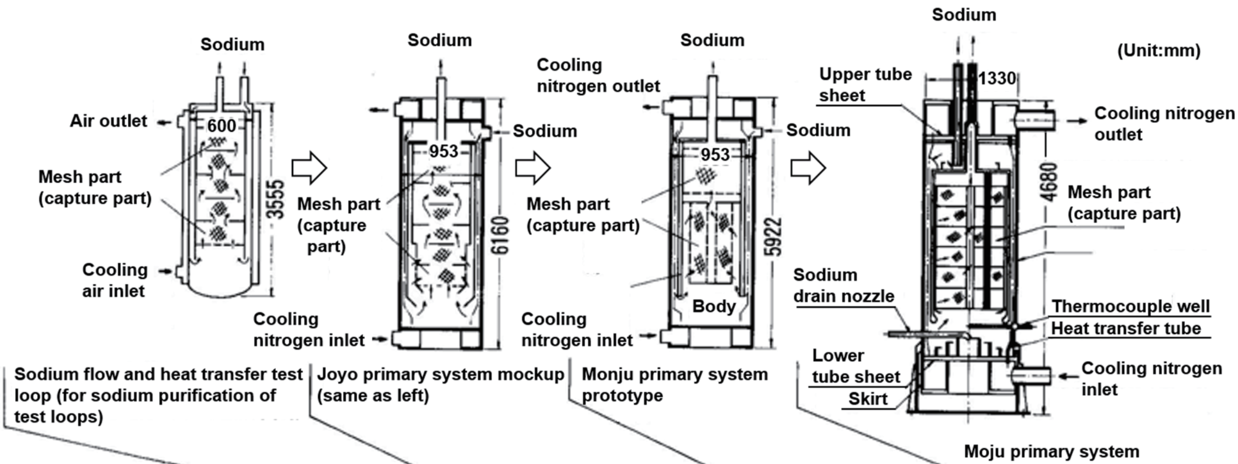

Impurity capture capacity	—— kg – O_2	16 kg – O_2	26 kg – O_2	70 kg – O_2
Test items	Purification characteristics, temperature distribution, operating characteristics Impurity capture capacity / capture distribution (overhaul)			Design evaluation using analysis code, etc.
Main structure	・Sodium flow path in mesh part: Small inflow area, long flow path → ・Temperature distribution in mesh part: Temperature rise along the flow → ・High mesh filling rate 200kg/m³		・Large inflow area, short flow path ・Uniform (with adiabatic gas layer) ・High mesh filling rate 200kg/m³	・Same as left ・Same as left ・Low mesh filling rate 100kg/m³
Findings or achievements (reflected to Monju)	・Impurities are trapped effectively in low-temperature regions. ・Uniform temperature distribution increases purification efficiency and capture capacity. ・Development of analysis code (CTRAP) ・Purification performance can be simulated. ・Cold trap design guidelines are established.		・Validation of design improvement ・Validation of analysis code ・Impurity trapping capacity can be increased by lowering mesh filling rate	・The same type of cold trap was installed in primary system of Joyo, and has already been operating smoothly.

Fig.8-2 Development of cold trap for Monju primary system

Joyo, as well as in foreign FRs. The determination of impurity becomes difficult when various types of impurities with different saturated solubilities are present in sodium (called the multiple breaking phenomenon).

(3) Sodium valves and bellows

Monju uses sodium valves in systems containing sodium and sodium vapor. A sodium valve needs to withstand high temperatures (200°C–550°C) and severe thermal transient conditions, and to have good sealing performance and corrosion resistance.

Special consideration must be given to the shaft sealing mechanism to prevent sodium leaks from sealed sections. The bellows seal and the freeze seal methods were adopted in Monju based on a variety of R&D activities.

The sodium valves are used in sodium test facilities and Joyo. The findings obtained in manufacturing and operating experience were integrated as a comprehensive technical guide on FR sodium valves. Large valves to be installed in the PHTS and SHTS were carefully developed through in-depth structural analyses, the manufacturing of prototypes, and function tests, in cooperation with valve and plant manufacturers.

The sizes of the bellows used in Monju vary from small to large, and the bellows were developed considering the specific conditions of sections to which they would be applied. For example, large bellows were used at the containment penetrations of the SHTS, and sealing bellows were used in the CRDMs and sodium valves. The bellows of frequently used valves and the CRDMs that have large strokes at a high speed were developed through cyclic fatigue tests to ensure high reliability.

8.3 Achievements in the commissioning

(1) Sodium purity control

The history of oxygen concentration in sodium, measured by the PL meter, in the PHTS since the commissioning (for about 20 years) of Monju is shown in Fig. 8-3. The CT in the PHTS has been operated at 130°C to keep the oxygen concentration at 3 ppm or lower (except for the initial purification period). At the beginning of operation, a short increase in the oxygen concentration due to the elution of oxygen attached to the surface of the structure associated with increased temperatures was observed. Thereafter, the oxygen concentration was appropriately controlled, demonstrating the required performance of both the CT and the PL meter. The sodium purity control in the SHTS was confirmed as well.

(2) CT performance

In the SHTS, it is important to keep the hydrogen concentration low during normal operation to ensure early detection of water leak from an SG tube. The purification efficiency in the design is 0.7. Figure 8-4 shows a change in hydrogen concentration when the operating temperature of the CT in the SHTS are changed in a ramp-wise manner. The response curve of the calculated hydrogen concentration agrees with the measured data when the purification efficiency is set at 0.85, which is better than the design value.

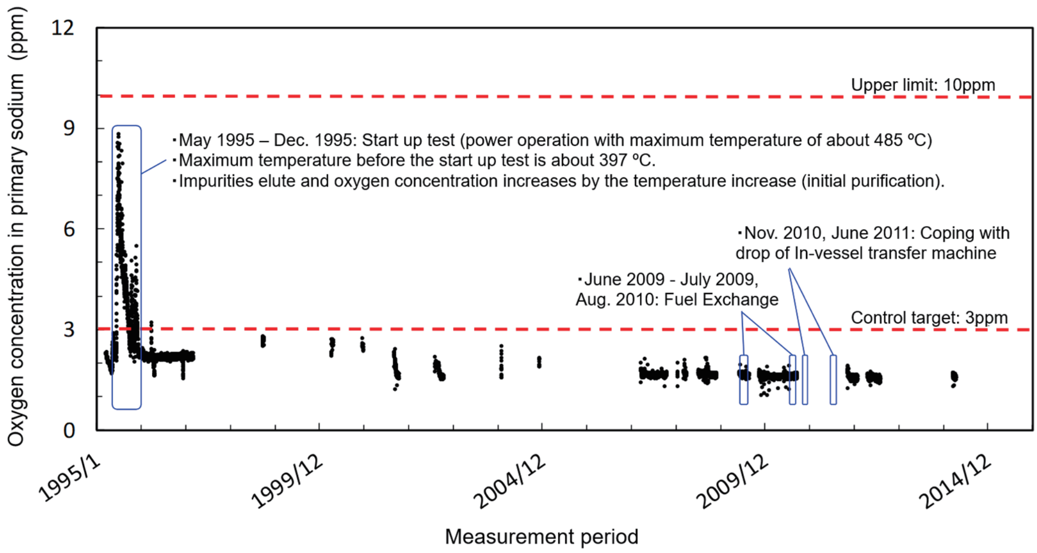

Fig.8-3 Trend of oxygen concentration in sodium in the primary cooling system

The primary and secondary system CTs both experienced incidents in which the impurities could not be temporarily removed during the initial purification operation phase. This was considered to have been caused by the poor sodium wettability of the mesh parts in the very early stage.

(3) Accumulation of experience in sodium cleaning

Monju has three cleaning systems: a spent fuel cleaning system, a cleaning system for the primary system components, and a cleaning system for the secondary system components. Sodium cleaning has been performed utilizing a combination of the steam cleaning (mixed with inert gas) and the water cleaning.

The alcohol cleaning was used specifically when the thermocouple sheath, the rupture of which was the cause of the Secondary Sodium Leak Accident, was cut out and subjected to material tests to determine the cause of the accident.

The experience of sodium cleaning in Monju is summarized in Table 8-1. The problems experienced in the spent fuel cleaning system were addressed to improve the system. The plant-level sodium cleaning technologies were established through these cleaning experiences.

8.4 Development of ISI technology

8.4.1 ISI policies and program

(1) Basic ISI policies

The basic ISI policies for Monju are as follows:

- The reactor coolant boundary is inspected by visual observation of welds and by sodium leak monitoring of the main components and piping throughout the in-service period.
- The reactor cover gas boundary is subjected to leak monitoring using radioactive cover gas monitors.
- The important structural materials undergo tests using a material surveillance piece. The environmental effects on the materials are assessed, as needed.

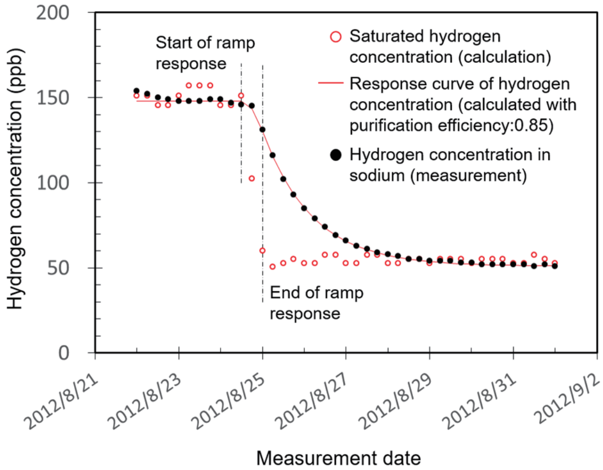

Fig.8-4 Purification efficiency of cold trap in the secondary cooling system

(2) Formulation of ISI program

The Monju ISI program was formulated in accordance with the basic ISI policies by consulting U.S. ASME Boiler & Pressure Vessel Code Case Sec. XI, Div. 3 (the rules for ISI of liquid-metal-cooled reactors). An overview of the ISI program for Monju is shown in Table 8-2. The

Table 8-1 Major experiences of sodium cleaning (up to July 2011)

Objects to be cleaned	Number	Cleaning method	Remarks
FCRD upper guide tube	3	Wet nitrogen gas cleaning + water cleaning + depressurized cleaning with hot water	-
Dummy fuel subassemblies, etc.	203	Wet argon gas cleaning + demineralized water cleaning	-
IVTM	1 set	Wet argon gas cleaning + demineralized water cleaning	-
Temporary strainer	3	Steam cleaning	-
Damaged temperature sensor sheath	1	Alcohol cleaning	Material test
Removed secondary sodium piping and valves	1 set	Wet nitrogen gas cleaning + water cleaning + circulated hot water cleaning	-
Leaked secondary sodium	-	Wet nitrogen gas cleaning + water cleaning + circulated hot water cleaning	Sodium deposited in piping room
Pressure relief plate for superheater	1	Alcohol cleaning	Material test

Table 8-2 Overview of ISI program

Component	Inspection items	Methods of inspection
RV	Surroundings of guard vessel	Visual inspection, sodium leak monitor, material surveillance
	Outside guard vessel	Sodium leak monitor, radioactive cover gas monitor
Shield plug	Reactor cover gas boundary	Visual inspection, sodium leak monitor, radioactive cover gas monitor
PHTS circulation pump	Outer casing	Visual inspection, sodium leak monitor, radioactive cover gas monitor
PHTS IHX	Shell	Visual inspection, sodium leak monitor
	Heat transfer tube	Leak monitor
PHTS piping	Piping	Visual inspection, sodium leak monitor, volumetric inspection
PHTS check valve	Valve box	Sodium leak monitor
Guard vessel	Shell	Visual inspection, (material surveillance)
Core support structure	Core support plate, core barrel	Material surveillance
Primary auxiliary sodium system piping	Piping	Sodium leak monitor
SHTS circulation pump	Outer casing	Visual inspection, sodium leak monitor
SG	Shell	Visual inspection, sodium leak monitor
	Heat transfer tube	Volumetric inspection
SHTS piping	Piping	Visual inspection, sodium leak monitor, volumetric inspection
Auxiliary cooling system air cooler	Heat transfer tube	Sodium leak monitor
Ex-vessel fuel storage system	Sodium boundary	Sodium leak monitor

program was based on R&D of inspection devices for RV visual testing and for the volumetric examination of the PHTS piping as well as the inspection programs of Joyo and LWRs along with the achievements thereof. The unique features of Monju were appropriately taking into account.

8.4.2 Development of inspection devices

(1) Inspection devices for RV and its surroundings

The visual inspection of the main RV parts and inlet piping are to be performed under the unprecedented conditions of a narrow space inside the guard vessel and high temperature and radiation environment. Therefore, a remote-controlled inspection device was newly developed adopting an environment-resistant remote visual sensor. For the RV, a device equipped with an electromagnetic acoustic transducer (EMAT) sensor for volumetric inspection was also developed for R&D purposes to detect small defects before they grow to penetrate the RV wall.

The newly developed inspection devices were applied to the visual tests of a pre-service inspection (PSI) of Monju. The absence of significant defect in the RV wall was confirmed, and several points of improvement were identified for inspection device operation.

To reduce the time for inspection and improve reliability and durability, the RV inspection device was modified by improving accessibility to narrow spaces, widening the field of view using a CCD camera, and reducing the maintenance time by improving the durability of mounted components while taking into account the experience obtained in tests performed in the initial development phase. The improvements in accessibility are illustrated in Fig. 8-5. The improved functions were checked in functional tests using a mockup system and the performance requirements were satisfied.

Meanwhile, the EMAT was further improved by enhancing signal strength and reducing size and weight by adopting the technologies developed in the field of accelerators. As a result, defects with a depth-to-plate thickness ratio of 20% were successfully detected with the new sensor. However, the problem of electrical noise arose when the sensor was mounted on the inspection device. Further improvement is needed for practical application.

(2) Inspection devices for PHTS piping

The ISIs for the PHTS piping include visual inspection and volumetric inspection. Since the technologies were already available for the visual inspection device, the development of a volumetric examination device focused on the available LWR technologies taking into account thin-walled, large-diameter piping specific to FRs.

One of the key features of the device is the use of a tire-type ultrasonic probe. In order to reduce worker exposure, non-couplant probes, not requiring a contact medium, were employed for continuous inspections in vertical and oblique angles.

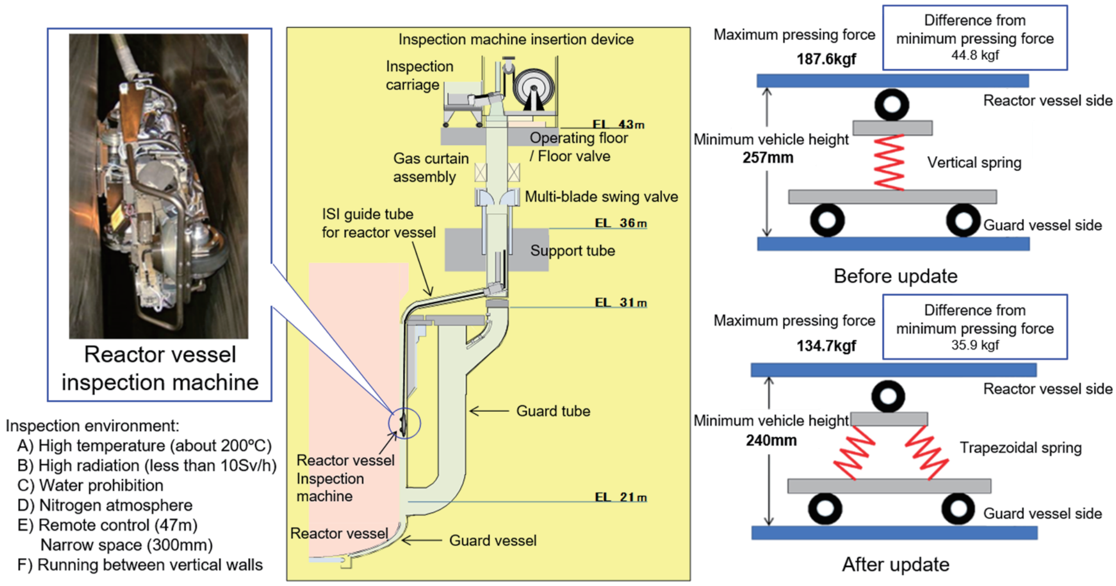

Fig.8-5 Improvement of accessibility in narrow space

In the function tests and PSI using the PHTS piping volumetric examination device, the inspection device demonstrated satisfactory performance in terms of driving, flaw detection, and data storing functions, while identifying remaining issues, such as the complexity of inspection procedure and the deterioration of sensitivity due to aging.

The tire-type probes and the scanner were further improved, and the control device and the data storage device were updated. The functions of the new system were confirmed in a mockup system and in the piping of Monju. The sensitivity and other probe performance were further improved on the basis of the obtained data.

(3) SG tube inspection device

The SG tubes have a complex structure with a long, helically-coiled shape (maximum length: 85 m). The evaporator tubes are made of a magnetic material, which is unsuitable for a conventional eddy current test (ECT). In addition, they have a thick wall, which is difficult for the eddy currents and magnetic fields to penetrate. Because of the above, the inspection technologies successfully used for LWRs could not be applied without modification. To address this, new inspection technologies were developed with a focus on the ECT for ferromagnetic and thick-wall piping.

In the function tests of the test device and PSI, information was obtained on a series of operational performance related to transfer, assembly, installation, adjustment, and flaw detection using the device. In addition, flaw detection data on all the heat transfer tubes in the evaporators and superheaters were collected for ISI.

The defect detection performance and the aligning mechanism were improved while noise reduction was achieved (Fig. 8-6). A multiple-frequency algorithm was also developed for improved signal processing. Performance was further improved to detect defects on the support structure with sodium attached to the outer surface of SG tubes. Evaporator flaw detection data were obtained in PKS, and stable and improved detectability was confirmed.

8.4.3 Integrity confirmation of SG tubes of Monju

Before resuming Monju operation following completion of the modification work after the Secondary Sodium Leak Accident, the integrity of the SG tubes, which had been in long-term storage, had to be confirmed. The SG tubes thus underwent a series of inspections over about five months from November 2007.

The SG tubes in the loops were subjected to ECT (all tubes), leak tests (all tubes), and visual tests (sampled tubes), and these results comprehensively confirmed the integrity of the SG tubes. The leak and visual tests were voluntarily performed to ensure that there was no influence on the tubes from long-term storage. The configuration of the ECT system is illustrated in Fig. 8-7. Photographs of the inner surface of an evaporator heat transfer tube are shown in Fig. 8-8. Although scale was observed on parts of

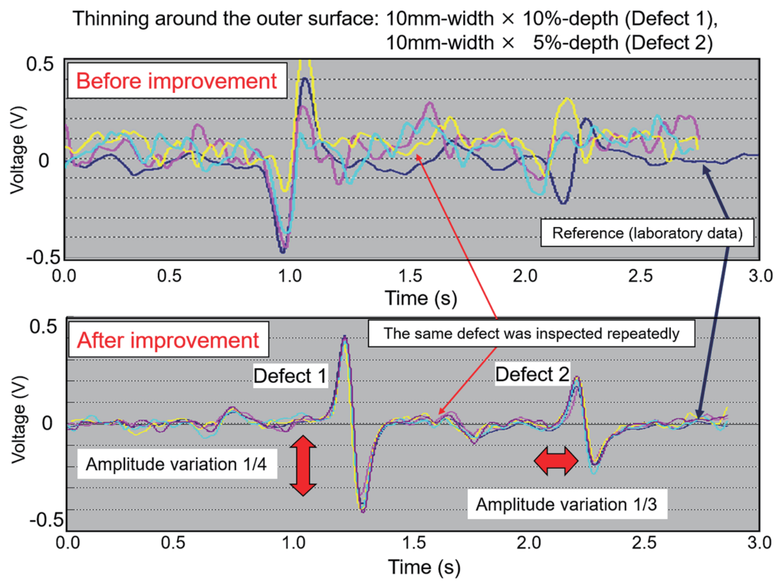

Fig.8-6 Defect detectability before and after vibration countermeasures (mockup test)

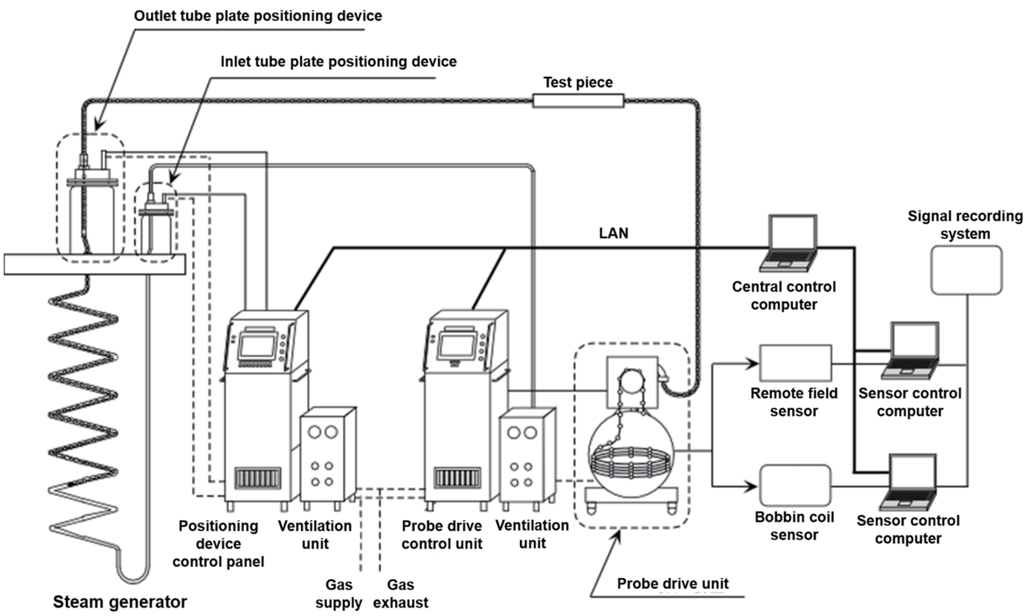

Fig.8-7 Configuration of eddy current test devices

the inner surface of the heat transfer tubes, no significant corrosion or other defects were found.

8.5 R&D related to CP

Iron, manganese and other elements contained in the FR core material that activate, elute, and migrate to the components and piping in the primary system, depositing and adhering to their surfaces, are called corrosion product (CP). During refueling the CP is transferred to the spent fuel cleaning system. In the overhaul inspections and repair of the primary system components, the CP is transferred to the liquid waste disposal facility. Since the CP becomes a radiation source, which is one of the major causes of exposure during facility maintenance, comprehensive measures against CP are required.

To address this problem, various tests and analyses of the data obtained in Joyo were per-

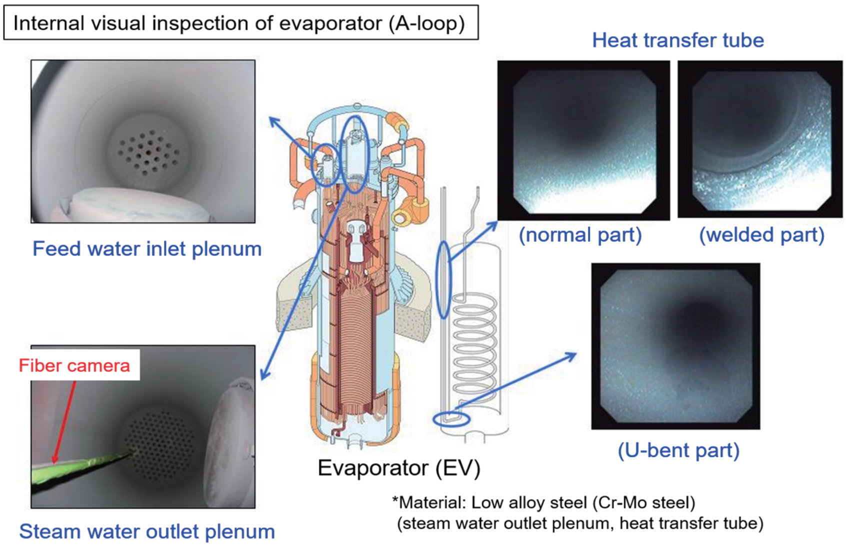

Fig.8-8 Internal visual inspection of evaporator

formed to develop analysis methods to evaluate CP behavior and suppression. Technologies were also developed to remove the CP deposited on and adhering to the components and piping.

(1) CP behavior analysis codes

A CP behavior analysis code, PSYCHE/JOANDARC, was developed to model the transport process consisting of the dissolution and deposition of the CP. The code was validated by comparing with the surface dose rate distribution and the CP deposition density on the PHTS piping measured in Joyo. Taking these results into account, the CP distribution behavior in Monju was predicted, and the effect of measures to reduce the CP was evaluated. Moreover, the dose rate estimation system for FR maintenance, DORE, which visualizes the dose maps, was developed for Monju. The FR tritium behavior analysis code TTT and the FP behavior analysis code SAFFIRE were later incorporated into the DORE system to create an integrated radiation dose evaluation tool.

The dose rate distribution by the saturated source terms in the PHTS room during the rated power operation of Monju was predicted using DORE, as shown in Fig. 8-9. The histories of the dose rates with reactor power operation were predicted in Fig. 8-10 on the surfaces of thermal insulator in snubber sections of the PHTS hot-leg and cold-leg pipings. It was predicted that the dose rate would be saturated before reaching a cumulative reactor power of 2,000 GWd (13-year operation) and the saturated dose rate in cold-leg would be 3 mSv/h, which is higher than the 2 mSv/h in hot-leg. Isotopes ^{54}Mn and ^{60}Co almost equally contribute to the dose rate in hot-leg, whereas ^{54}Mn is dominant in cold-leg. These achievements enable the accurate prediction of dose rates during maintenance and inspection. A better understanding of the radiation environment in a comprehensive and intuitive manner is useful in the design of measures to reduce radiation exposure.

(2) CP suppression

The generation of CP can be suppressed by reducing the CP sources and removing the CP in a CP trapping device. In the reduction of the CP sources, isotope ^{60}Co, a major source of exposure, was reduced by developing a non-cobalt-base (cobalt-free) surface hardening material instead of Stellite alloy comprising in more than 50% cobalt, generally used as a surface hardening material on the sliding parts (e.g., pump bearing) of a device in order to improve wear resistance. The other major source of ^{54}Mn is difficult to reduce effectively since it is yielded mainly from ^{54}Fe originally contained in stainless steel. Then a CP trapping device using a nickel getter material was developed to trap ^{54}Mn. The performance of the device was confirmed in out-of-pile tests and Joyo. Based on the test results, the prospect for application of the device to Monju became clearer.

(3) CP decontamination

Technologies to decontaminate the CP were developed through basic tests, small-scale tests, and actual component decontamination tests using the Fuel Monitoring Facility of the

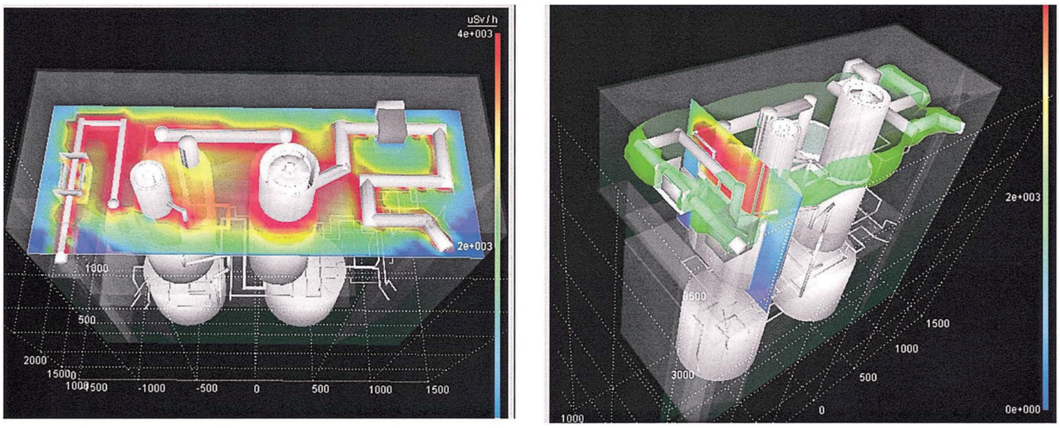

Fig.8-9 Radiation dose rate map in primary heat transport system room[8-3)]

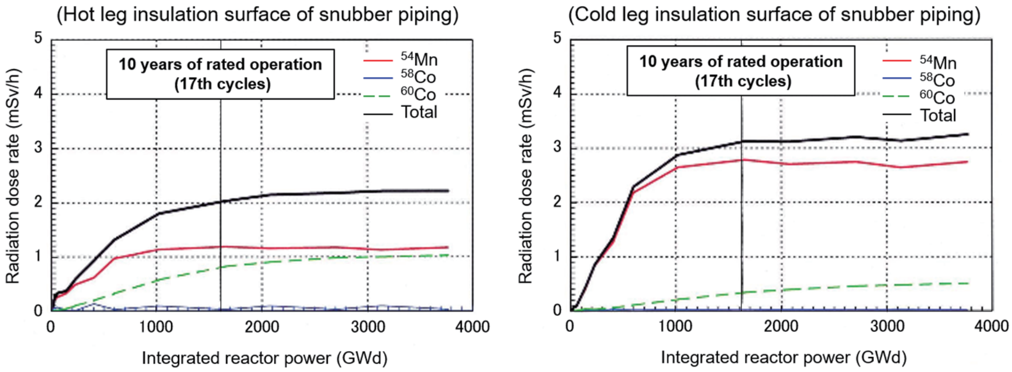

Fig.8-10 Predicted radiation dose rate for the primary cooling system at the rated power operation

OEC and the spent fuel cleaning system in Joyo. The target values of sufficient decontamination factors were attained by these tests and the dose rates were reduced accordingly. Technologies to chemically decontaminate the CP adhering to the spent fuel cleaning system were developed as well. The most suitable decontaminant and decontamination conditions were selected using the actual plant piping, and small-scale tests using an out-of-pile loop and actual plant tests in Joyo were carried out. As a result, the piping and component surface dose rates were halved. Through these efforts, chemical decontamination technologies applicable to the FR spent fuel cleaning systems were established.

(4) CP removal

Concerning technologies to remove the CP, the properties of the waste water discharged in cleaning the fuel and components used in Joyo were analyzed to clarify their basic conditions and behavior. In addition, the validity of a CP removal system based on a vitrification method was proven through modification and operation evaluation of the liquid waste disposal facility for the Joyo fuel.

— References —

8-1) Power Reactor and Nuclear Fuel Development Corporation, Fast Breeder Reactor, PNC-TN9520 91-006, 1991 (in Japanese).
8-2) Yoshida, E. et al., Accumulation of Experiences and Knowledge for Sodium Cleaning Treatment Technology, JAEA-Technology 2012-033, 2012, 177p. (in Japanese).
8-3) Iizawa, K. et al., Development of Dose Rate Estimation System for FBR Maintenance, JNC Technical Review, No. 12, JNC-TN1340 2001-007, 2001, pp.21-36 (in Japanese).